รายงานฉบับสมบูรณ์

การเลี้ยงเชื้อมาลาเรียชนิดไวแว็กซ์อย่างต่อเนื่องด้วยการใช้เซลล์เม็ด เลือดแดงตัวอ่อนที่ผลิตโดยการเลี้ยงและแยกเซลล์ต้นกำเนิดด้วย high-gradient magnetic separation (BRG5380006)

ศ.ดร. รัชนีย์ อุดมแสงเพ็ชร

ภาควิชาพยาธิชีววิทยา คณะวิทยาศาสตร์ มหาวิทยาลัยมหิดล

บทคัดย่อ

ความพยายามในการแยกและเลี้ยงเซลล์ตันกำเนิดของเม็ดเลือดแดงจากเลือดสายสะดือเด็กแรกเกิดนั้น ได้ผลดี เมื่อทำการแยกด้วยอุปกรณ์ที่มีขายด้วยการนำเข้าจากต่างประเทศ การแยกเซลล์โดยอาศัยแรง ดึงดูดของแม่เหล็กให้มีประสิทธิภาพสูงนั้นต้องใช้วิธีการจับเซลล์นั้นด้วยสารที่มีความจำเพาะต่อโมเลกุล บนผิวของเซลล์นั่นคือ การใช้แอนติบอดีที่ติดไว้กับparamagnetic nanobead แต่ในปัจจุบันนี้ยังขาด การศึกษาและความรู้ในลักษณะและคุณภาพของการจับติดกันระหว่างเซลล์กับnanobead ในราย งานวิจัยนี้จึงศึกษาอัตราการจับติดกันทั้งแบบที่มีและไม่มีความจำเพาะต่อกัน ปริมาณของnanobead ที่จับอยู่บน ผิวเซลล์สามารถวัดได้ด้วยspectrophotometry แสดงผลให้เห็นว่าอัตราการจับของnanobead กับเซลล์ ตั้งแต่ระยะเริ่มตันจนถึงระดับอิ่มตัวนั้นสัมพันธ์กับความเข้มขันของnanobeadที่ใช้ ส่วนในการทดสอบ แยกเซลล์เม็ดเลือดขาวชนิดCD3+นั้นพบว่าโอกาสที่จะเกิดการจับกันระหว่างเซลล์กับnanobead นั้นมี สูงถึง 80 เท่าตัวเมื่อเทียบกับการจับแบบไม่จำเพาะ

ประการต่อมาคือการแยกชนิดเม็ดเลือดแดงตัวอ่อนออกจากกันเพื่อใช้เลี้ยงเชื้อมาลาเรียชนิด P.vivax นั้น ยังไม่สามารถทำให้ antibody ที่ต้องการไปติดอยู่บน nanobead ได้ จึงไม่มีคุณภาพดีพอมาใช้งาน แยกเซลล์ดังกล่าวได้ ในงานส่วนนี้ยังทำไม่สำเร็จ

Keywords: high gradient magnetic separation; bead-cell binding; iron content; paramagnetic nanoparticles, magnetic labelling, cell separation

Abstract

An attempt to isolate and cultivate hematopoietic stem cells from cord blood has been successful considering the application of a commercialized antibody-conjugated nanobeads imported from other countries. Specific labelling of target cell surfaces using antibody-conjugated paramagnetic nanobeads is essential for efficient magnetic cell separation.

However, studies examining parameters determining the kinetics of bead-cell binding are scarce. The present study determines the binding rates for specific and unspecific binding of 150 nm paramagnetic nanobeads to highly purified target and non-target cells. Beads bound to cells were enumerated spectrophotometrically. Results show that the initial bead-cell binding rate and saturation levels depend on initial bead concentration. Unspecific binding within conventional experimental was not detectable photometrically. For CD3-positive cells, the probability of specific binding was found to be around 80 times larger than that of unspecific binding.

However, the second part of this project attempting to isolate various stages of erythrocytes from cultivated hematopoietic stem cells in order to serve as new target cells for *P.vivax* malaria parasite is not successful. Due to the fact that the selected antibody used in conjugation with the nanobead did not render a satisfactory amount of the cells and neither the specific cell isolation. Therefore, the attempt to cultivate *P.vivax* malaria parasite in vitro is not successful.

Keywords: high gradient magnetic separation; bead-cell binding; iron content; paramagnetic nanoparticles; magnetic labeling; cell separation

Executive Summary

การเลี้ยงเชื้อมาลาเรียชนิดไวแว็กซ์อย่างต่อเนื่องด้วยการใช้เซลล์เม็ดเลือดแดงตัวอ่อนที่ผลิต โดยการเลี้ยงและแยกเซลล์ตันกำเนิดด้วยhigh-gradient magnetic separation

Development of continuous culture of *Plasmodium vivax*: Modified procedures using erythroblasts isolated from human hematopoietic stem cells by high-gradient magnetic separation.

Rationale of the study

Plasmodium falciparum and Plasmodium vivax are the two most prevalent human malaria parasites. In recently years, P. vivax has become a major public health problem in many regions of the world (Mendis et al., 2001; Sattabongkot et al., 2004). Thailand is one of the malaria-endemic countries where P. vivax has become the most prevalent human malaria parasite. Chloroquine-resistant P. vivax strains have been reported in many P. vivax-endemic regions (Rieckmann et al., 1989; Baird et al., 1996). In addition, understanding of the host immunity to P. vivax infection is scanty due to the lack of parasite materials for in vitro studies. Although recent efforts in culturing P. vivax have led to the development of a short-term culture method (Chotivanich et al., 2001), establishment of a continuous in vitro culture system for this parasite proves very difficult. A major obstacle is the selective invasion of erythroblast by the parasite (Panichakul et al., 2007). Therefore, continuous in vitro cultivation of the P. vivax parasite depends on the unlimited production of erythroblastic cells to serve as host cells. Several successful attempts to cycle P. vivax in continuous culture used reticulocyte-enriched blood either from monkeys that were treated with a hemolytic drug (Mons et al., 1988), or from hemochromatosis patients (Golenda et al., 1997), or from human cord blood (Udomsangpetch et al., 2007; Udomsangpetch et al., 2008). However, these procedures have received very limited applications in P. vivax research due to its labor-intensiveness and the unavailability of reticulocyte-enriched human blood.

Research in *P. vivax* malaria often requires *in vitro* manipulations of the parasite field isolates for more extended period. In recognition of this need and based on the techniques we recently report (Panichakul et al. 2007); we therefore propose to develop a modified procedure for unlimited production of human erythroblasts to maintain the continuous culture of *P. vivax*. The materials produced by the in vitro cultivation of *P. vivax* will support abundant number of projects that have not been studied in this malaria parasite over the past decades. The products of this project will enhance various studies of *P. vivax* in different geographic regions, and significantly strengthen the success of several other researchers of the malaria community.

Objectives

- Produce human hematopoietic stem cell line to provide unlimited erythroblasts for research use.
- 2. Develop a simple and low cost cell separation technique for hematopoietic stem cells.
- 3. Establish a continuous culture line of P. vivax parasite.

Methods

Part I – Production of erythroblastic cells

A.1. Isolation and production of hematopoietic stem cells from human cord blood

Human umbilical cord blood samples obtained from Ramathibodi Hospital will be used for hematopoietic stem cell (HSCs) isolation. Cord blood collection (ID 04-45-16, see Appendix) has been approved by the Ethical Committee of Research on Human Being from Ramathibodi Hospital, Faculty of Medicine, Mahidol University, Bangkok, Thailand.

A.2. Separation of mononuclear cells and isolation of stem cells

Mononuclear cells (MNCs) from cord blood will be separated by LymphoPrep solution (Schlenke et al. 1998). The CD133⁺ hematopoietic stem cells (HSCs) will be isolated by magnetic microbead selection, and Mini-MACS columns (Miltenyi Biotech,Germany) then cultured with Stemline II medium in 6-well plate for producing gRBCs.

A.3. Isolation of HSCs by high gradient magnetic separation (HGMS)

HGMS technology (Bhakdi&Malasit 2007) is adapted for use with hematopoietic stem cells and erythroblastic cells. The HGMS device consists of a horseshoe magnet, a separation column, and a fluid reservoir. HSC are labelled with magnetic microbeads as described above and separated by the HGMS separating column.

A.4. Propagation of hematopoietic stem cells

HSCs/CD133⁺ cells will be cultured in Stemline II medium supplemented with stem cell factor, IL-3, hydrocortisone, transferring, humulin[®] N, ferrous sulfate, monothioglycerol. The cells will be diluted with the complete Stemline II medium every 4 days for expansion of the HSC. The HSC are cultured in Stemline II medium with transferrin, humulin[®] N, ferrous sulfate, monothioglycerol and erythropoietin (EPO) for production of erythroblastic cells. All cultures will be incubated in the CO₂ incubator at 37 \square C with 5% CO₂.

A.5. Determination of the culture quality and analysis of cell differentiation

Discontinuous gradients (30-60%) of Percoll (Sigma-Aldrich, Inc, USA) are used to separate heterogeneous cell populations from the cell culture on day 10. Each cell fraction is separated, washed twice with RPMI medium by centrifugation at 1,000 g for 10 min. Differential enumeration of each cell type is performed by morphological examination of Giemsa's stained cells using light microscope (Olympus BX50, Japan).

B. Isolation and production of hematopoietic stem cells from induced pluripotent stem cells

B.1. Induced pluripotent stem cells (IPS)

Production of hematopoietic stem cells is modified from Ye et al. 2009. In our system, induction of human fibroblasts is performed by co-transfection with pMXs retroviral vectors, containing the human genes Oct3/4, Sox2, Klf4, c-Myc, Nmyc, Nanog, and Lin28 (Addgene). Early erythroblastic cells will be enriched by buffer optimized HGMS.

Part II - Cultivation, isolation and characterisation of P.vivax-infected red blood cells

Patient recruitment

Patients with *P. vivax* parasitemia visiting the Malaria Clinic in Mae Sot district, Tak province are recruited to the project. The human use protocol has been approved by the Ethical Review Committee of Mahidol University. Parasite infection is confirmed by microscopic examination of thin and thick blood films. After informed consent is obtained, 5 ml of blood are withdrawn into a heparinized tube.

Parasite cultures

P.vivax-infected red blood cells at mature stages, i.e. schizonts, are enriched by 60% Percoll gradient separation techniques. The parasites and erythroblast are mixed and cultured as described by Panichakul et al. 2007. Parasitemia and maturation are determined by Giemsa's staining of thick blood films.

References.

Bhakdi SC & Malasit P (2007). Hochgradientenmagnetseparation biologischen Materials. Patent filing no. DE 10 2007 043 281.1, *German Patent Office*. (Dependent patents filed at the Thai and European Patent Office.)

Chotivanich K, Silamut K, Udomsangpetch R, Przybylska KA, Pukrittayakamee S, Looareesuwan S, White NJ, 2001. Ex-vivo short term culture and developmental assessment of *Plasmodium vivax*. Trans R Soc Trop Med Hyg 95:677-680.

Golenda CF, Li J, Rosenberg R, 1997. Continuous *in vitro* propagation of the malaria parasite *Plasmodium vivax*. Proc Natl Acad Sci USA 94:6786-6791.

Mendis KN, Sina BJ, Marchesini P, Carter R, 2001. The neglected burden of *Plasmodium vivax* malaria. Am J Trop Med Hyg 64:97-106.

Mons B, Collins WE, Skinner JC, van der Star W, Croon JJAB, van der Kaay HJ, 1988. *Plasmodium vivax*: In vitro growth and reinvasion in red blood cells of *Aotus nancymai*. Exp Parasitol 66:183-188.

Panichakul T, Sattabongkot J, Chotivanich K, Sirichaisinthop J, Cui L, Udomsangpetch R. 2007. Production of erythropoietic cells in vitro for continuous culture of *Plasmodium vivax*. Intl J Parasit 37:1551-1557.

Rieckmann KH, Davis DR, Hutton DC,1989. *Plasmodium* vivax resistance to chloroquine? Lancet 2:1183-1184.

Sattabongkot J, Tsuboi T, Zollner GE, Sirichaisinthop J, Cui L, 2004. *Plasmodium vivax* Transmission: Chances for Control? *Trends Parasitol* 20:192-198.

Udomsangpetch R, Somsri S, Panichakul T, Chotivanich K, Sirichaisinthop J, Yang Z, Cui L, Sattabongkot J. 2007. Short-term *in vitro* culture of field isolates of *Plasmodium vivax* using umbilical cord blood. Parasit Intl 56:65-69.

Udomsangpetch R, Osamu K, Chotivanich K, Sattabongkot J, 2008. Cultivation of *Plasmodium vivax*. Trend Parasitol 24:85-88.

Ye L, Chang JC, Lin C, Sun X, Yu J, Kan YW, 2009. Induced pluripotent stem cells offer new approach to therapy in thalassemia and sickle cell anemia and option in prenatal diagnosis in genetic diseases. *Proc Natl Acad Sci U S A* 106(24):9826-30.

ผลงานวิจัยที่ทำในรอบปี ประกอบด้วย

ผลงานวิจัยที่ส่งตีพิมพ์ 2 เรื่อง

 Shahid Waseem, Michael A. Allen, StefanSchreier, Rachanee Udomsangpetch,
 Sebastian C. Bhakdi*. Antibody-conjugated paramagnetic nanobeads: Kinetics of bead-cell binding. Int. J. Mol. Sci. 2014, 15, 8821-8834; doi:10.3390/ijms15058821 การแยกเซลล์โดยอาศัยแรงดึงดูดของแม่เหล็กให้มีประสิทธิภาพสูงนั้นต้องใช้วิธีการจับเซลล์นั้นด้วยสาร ที่มีความจำเพาะต่อโมเลกุลบนผิวของเซลล์นั้นคือ การใช้แอนติบอดีที่ติดไว้กับparamagnetic nanobead แต่ในปัจจุบันนี้ยังขาดการศึกษาและความรู้ในลักษณะและคุณภาพของการจับติดกันระหว่าง เซลล์กับnanobead ในรายงานวิจัยนี้จึงศึกษาอัตราการจับติดกันทั้งแบบที่มีและไม่มีความจำเพาะต่อกัน ระหว่างparamagnetic nanobead ขนาด 150 nm กับเซลล์ที่มีและไม่มีความจำเพาะต่อกัน ปริมาณของ nanobead ที่จับอยู่บนผิวเซลล์สามารถวัดได้ด้วยspectrophotometry แสดงผลให้เห็นว่าอัตราการจับ ของnanobead กับเซลล์ตั้งแต่ระยะเริ่มต้นจนถึงระดับอิ่มตัวนั้นสัมพันธ์กับความเข้มขันของnanobeadที่ ใช้และfit curves ของสมการ A(1-exp(-kt)) แต่การวัดระดับการจับแบบไม่จำเพาะภายในระยะเวลา 60 นาทีที่ทำการทดลองนั้นไม่สามารถวัดด้วยวิธีspectrophotometry นี้ ในการทดสอบแยกเซลล์เม็ดเลือด ขาวชนิดCD3+นั้นพบว่าโอกาสที่จะเกิดการจับกันระหว่างเซลล์กับnanobead นั้นมีสูงถึง 80 เท่าตัวเมื่อ เทียบกับการจับแบบไม่จำเพาะ

Keywords: high gradient magnetic separation; bead-cell binding; iron content; paramagnetic nanoparticles, magnetic labelling, cell separation

2. Shahid Waseem, Rachanee Udomsangpetch, Sebastian C. Bhakdi.

Buffer optimized high gradient magnetic separation: Collision theory predicts target cell capture rates. Submitted to Journal of Immunological Methods in 2013. (The present manuscript has investigated the effect of bead concentration and target cell concentration on the capture rate of CD14 positive cells and CD3 positive cells. The study also provides insight into the effect of bead size on capture rates in high gradient magnetic cell separation. Building on the insights of this study, improved protocols for HGMS isolation of cells with low antigen expression, like certain groups of stem cells, can be developed.)

However the Editor informed us that they could not find any Reviewer for the manuscript (The letter from the Editor is enclosed below.)

Sebastian Punyaratabandhu Bhakdi <sbhakdi@gmail.com>

Your Submission

Samuel Bader <jmmm@anl.gov> 21. August 2014 um 02:28

An: sbhakdi@gmail.com

Ms. Ref. No.: MAGMAD1300540

Title: Buffer optimized high gradient magnetic separation: target cell capture efficiency is

predicted by linear bead capture theory.

"Journal of Magnetism and Magnetic Materials"

Dear Dr.Med. Sebastian Chakrit Bhakdi,

I apologize for the serious delay in the review process of your manuscript. We have been unable to find reviewer to provide a review of your manuscript. Therefore we are returning it to you so that you can submit to a journal in your reference list where it will

reach an appropriate audience.

Thank you for giving us the opportunity to consider your work.

Yours sincerely,

Samuel D. Bader

Editor

Journal of Magnetism and Magnetic Materials

For further assistance, please visit our customer support site at

http://help.elsevier.com/app/answers/list/p/7923. Here you can search for solutions on a range of topics, find answers to frequently asked questions and learn more about EES via interactive tutorials. You will also find our 24/7 support contact details should you

need any further assistance from one of our customer support representatives.

การดำเนินงานในรอบปีที่ผ่านมา

พยายามสรรหา Antibody ที่มีอยู่เพื่อการใช้ในงานแยกเม็ดเลือดแดงตัวอ่อนต่อไป แต่ยังหา ไม่ได้ ถึงแม้เราทำการแยกและเลี้ยงเม็ดเลือดแดงตัวอ่อนได้ดีระดับหนึ่งแล้ว แต่การแยกชนิดเม็ดเลือด แดงตัวอ่อนแต่ละระยะออกจากกันเพื่อการเลี้ยงเชื้อ Plasmodium vivax นั้นทำได้ยากหากไม่มี

Antibody ที่จำเพาะต่อเซลล์ระยะดังกล่าว

Dr. Sebastian ผู้รับผิดชอบด้านการผลิต nanobeads เพื่อติดกับ antibody ที่จำเพาะต่อเม็ด

เลือดแดงตัวอ่อนก็ยังพัฒนาไม่สำเร็จดังคาดไว้

10

ผลที่ได้รับจากทดลองการเลี้ยงเม็ดเลือดแดงตัวอ่อน

การเลี้ยงและเตรียมเม็ดเลือดแดงตัวอ่อน

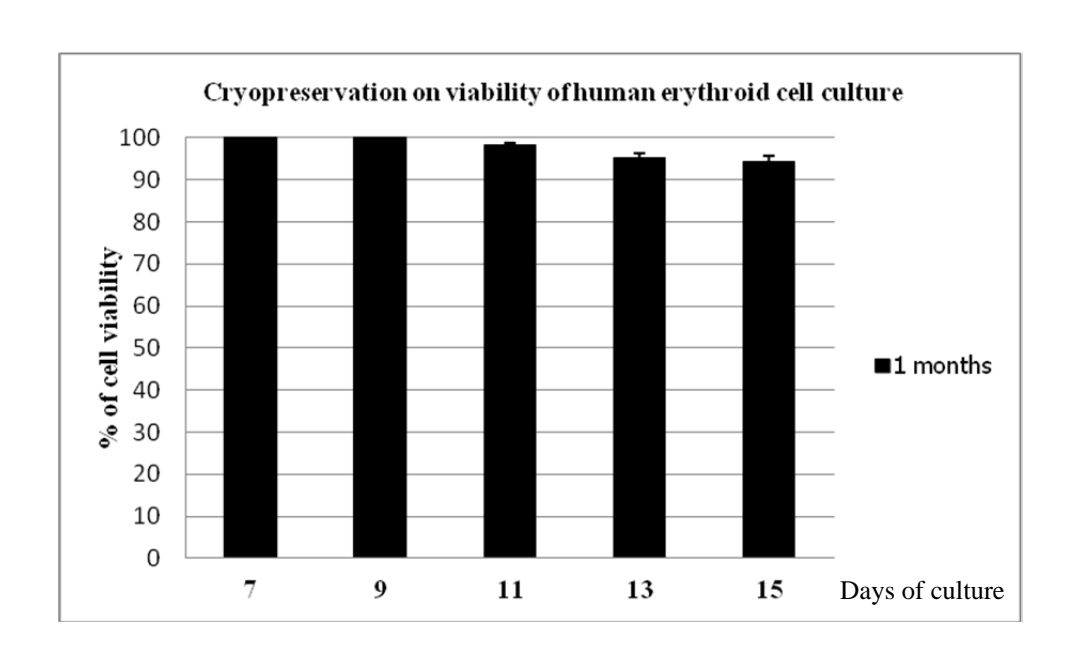
การทดสอบการเก็บเม็ดเม็ดเลือดแดงตัวอ่อนอายุ7วันของการเพาะเลี้ยง เก็บไว้ในถังแช่แข็ง (Liquid nitrogen) ในระยะเวลาต่างๆกัน ผลการศึกษาพบว่า ภายหลังจากการที่เก็บเซลล์ไว้เป็น ระยะเวลา ตั้งแต่ 1 เดือนถึง 6 เดือน พบว่าปริมาณเซลล์ที่มีชีวิตอยู่ 100% แต่ถ้าหากเก็บไว้ถึง 1 ปี พบปริมาณเซลล์ที่มีชีวิตอยู่ 97.06±1.42%

ส่วนการเจริญเติบโตของเซลล์ภายหลังแช่แข็งและทำการเพาะเลี้ยงต่ออีกหนึ่งสัปดาห์นั้นพบว่าเซลล์ เหล่านี้เจริญได้ดี และมี viability ดี

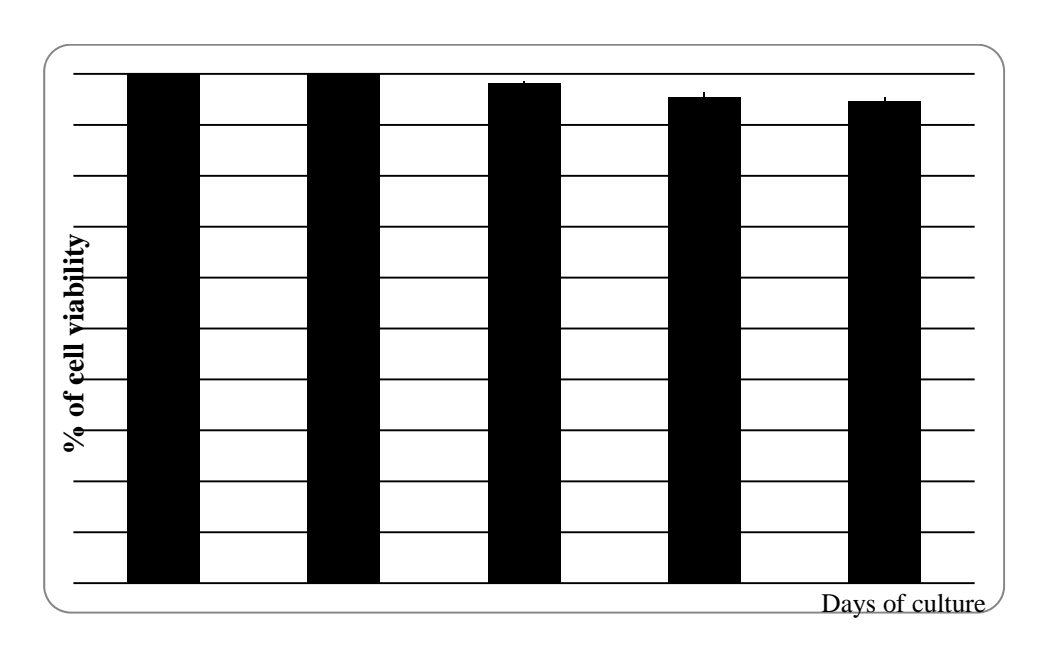
ตารางแสดงผลการทดสอบการเก็บเม็ดเม็ดเลือดแดงตัวอ่อนแช่แข็ง (Liquid nitrogen) ในระยะเวลา ต่าง ๆกัน

Time (months)	% of cell viability during re-cultivation post cryopreservation							
	Day 7	Day 9	Day 11	Day 13	Day15			
1	100	100	98.24 <u>+</u> 0.42	95.3 <u>+</u> 0.89	94.41 <u>+</u> 1.29			
3	100	100	98.15 <u>+</u> 0.38	95.45 <u>+</u> 0.85	94.67 <u>+</u> 0.62			
6	100	97.99 <u>+</u> 0.82	96.45 <u>+</u> 0.95	94.72 <u>+</u> 0.42	93.66 <u>+</u> 0.93			
12	97.06 <u>+</u> 1.42	96.05 <u>+</u> 0.79	92.39 <u>+</u> 0.82	90.78 <u>+</u> 0.82	87.52 <u>+</u> 0.95			

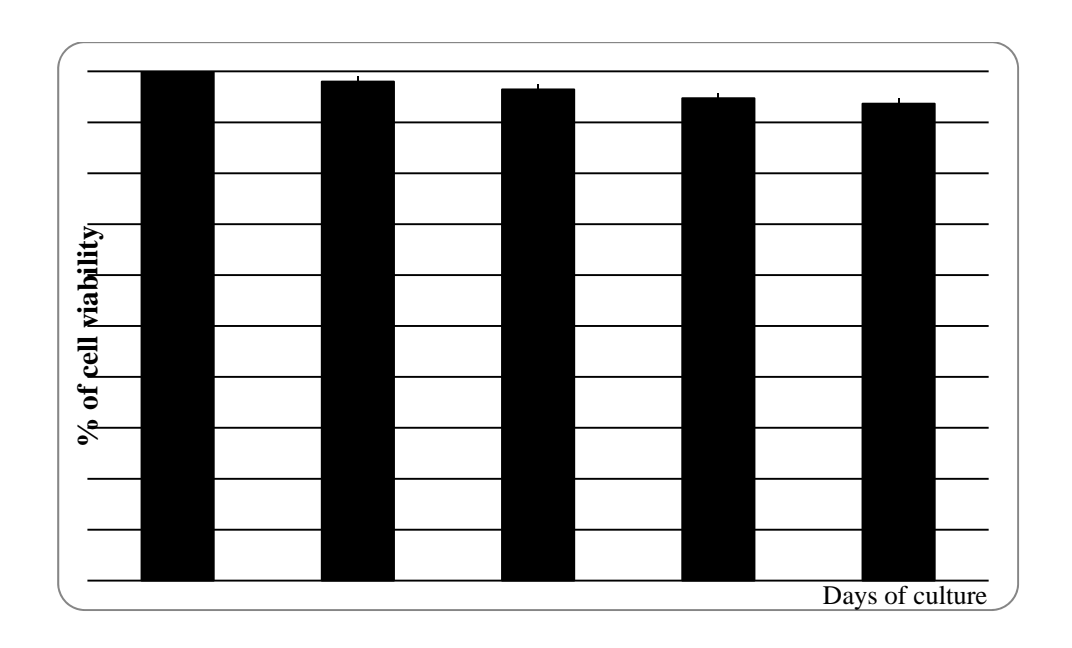
<u>กราฟที่ 1</u> แสดงผลการเก็บเม็ดเลือดแดงตัวอ่อนแช่แข็ง (Liquid nitrogen) เป็นเวลา 1 เดือนและ เพาะเลี้ยงเซลล์ต่อเนื่องหนึ่งสัปดาห์



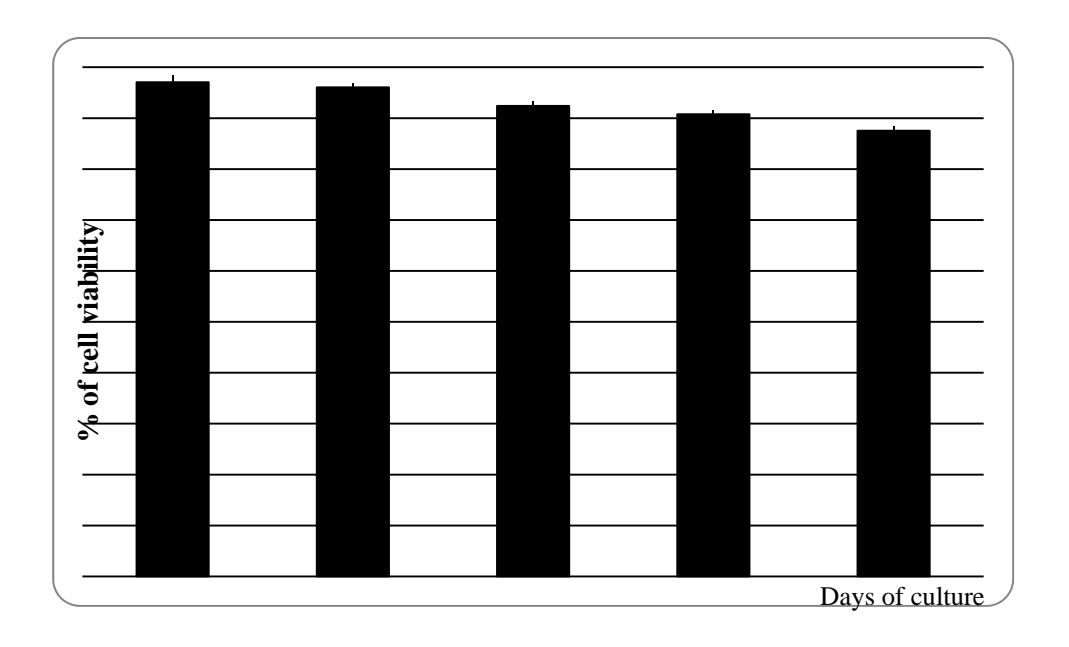
<u>กราฟที่ 2</u> แสดงผลการเก็บเม็ดเลือดแดงตัวอ่อนแช่แข็ง (Liquid nitrogen) เป็นเวลา 3 เดือนและ เพาะเลี้ยงเซลล์ต่อเนื่องหนึ่งสัปดาห์



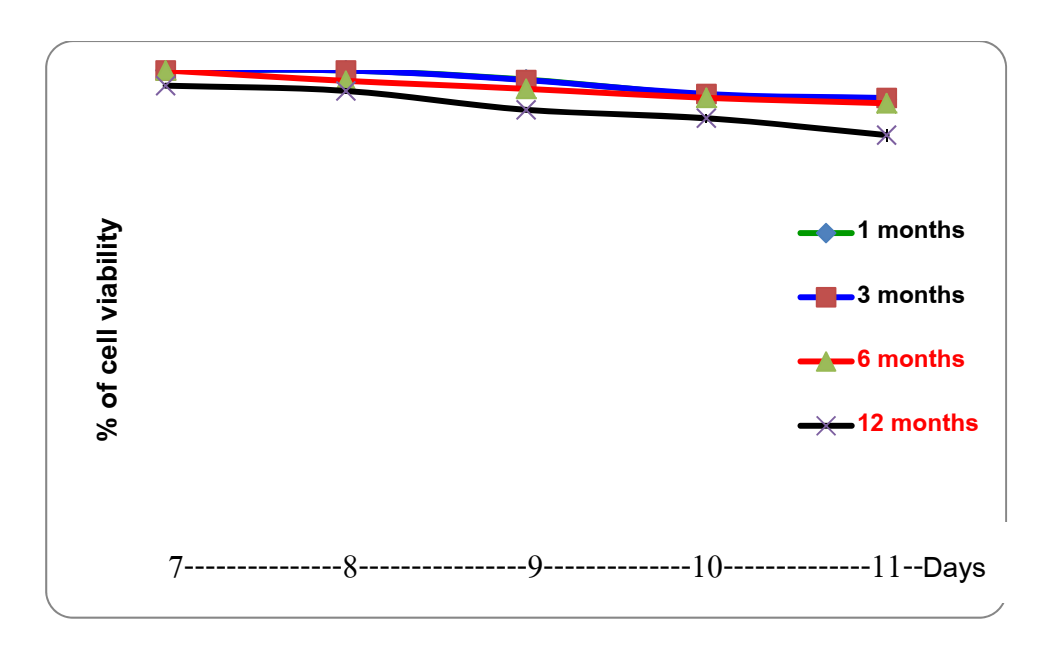
<u>กราฟที่ 3</u> แสดงผลการเก็บเม็ดเลือดแดงตัวอ่อนแช่แข็ง (Liquid nitrogen) เป็นเวลา 6 เดือนและ เพาะเลี้ยงเซลล์ต่อเนื่องหนึ่งสัปดาห์



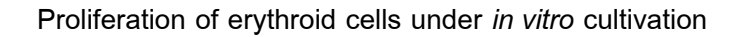
<u>กราฟที่ 4</u> แสดงผลการเก็บเม็ดเลือดแดงตัวอ่อนแช่แข็ง (Liquid nitrogen) เป็นเวลา 12 เดือนและ เพาะเลี้ยงเซลล์ต่อเนื่องหนึ่งสัปดาห์

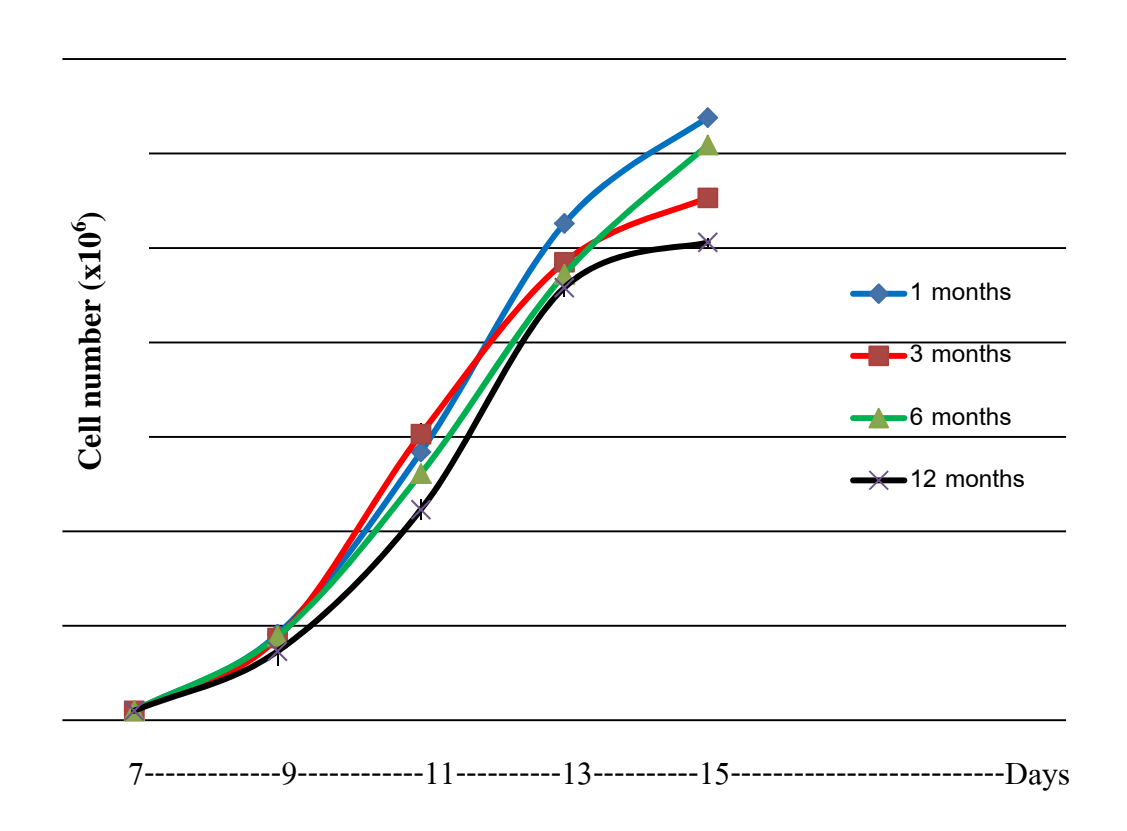


<u>กราฟที่ 5</u> แสดงการเปรียบเทียบviability ของเม็ดเลือดแดงตัวอ่อนอายุ 7 วันหลังจากการเก็บเซลล์ไว้ใน ถังแช่แข็ง (Cryopreservation in liquid nitrogen) นาน 1, 3, 6 และ12 เดือน และเพาะเลี้ยงเซลล์ ต่อเนื่องหนึ่งสัปดาห์ พบว่าไม่มีความแตกต่างกัน และการแช่แข็งเซลล์เช่นนี้มีคุณภาพดี Viability of human erythroid cells in the culture post cryopreservation



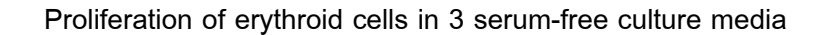
กราฟที่ 6 แสดงปริมาณเปรียบเทียบการเจริญเพิ่มจำนวนของเม็ดเลือดแดงตัวอ่อนที่เพาะเลี้ยงหลังจาก การเก็บเซลล์อายุ 7 วันไว้ในถังแช่แข็ง (Cryopreservation in liquid nitrogen) นาน 1, 3, 6 และ12 เดือน

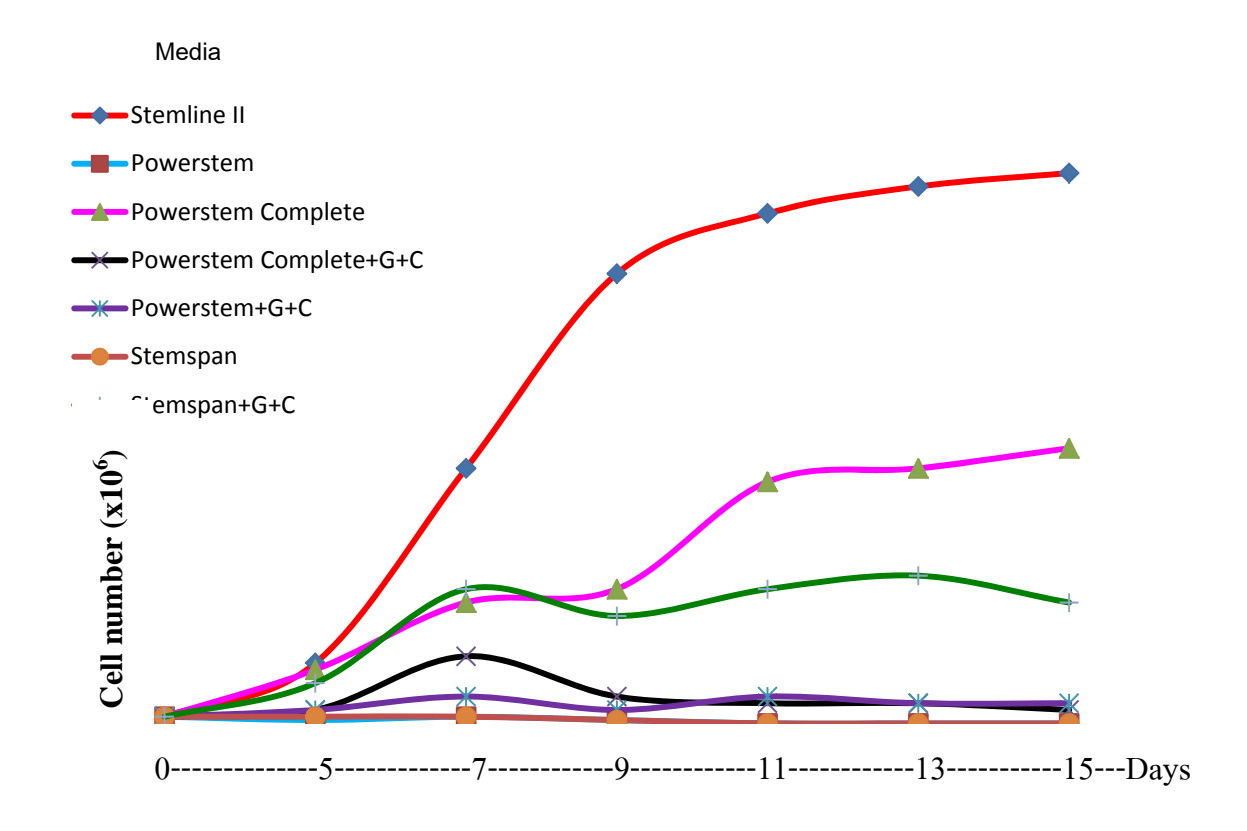




Time (months)	Cell Number (x10 ⁶)							
	Day7	Day9	Day11	Day13	Day15			
1	1	9.1 <u>+</u> 0.24	28.4 <u>+</u> 0.89	52.6 <u>+</u> 1.24	63.8 <u>+</u> 1.1			
3	1	8.7 <u>+</u> 1.19	30.3 <u>+</u> 1.12	48.5 <u>+</u> 0.46	55.3 <u>+</u> 0.53			
6	1	8.9 <u>+</u> 0.23	26.1 <u>+</u> 0.67	47.2 <u>+</u> 0.12	60.9 <u>+</u> 0.87			
12	1	7.3 <u>+</u> 1.52	22.3 <u>+</u> 1.1	45.8 <u>+</u> 0.93	50.6 <u>+</u> 0.47			

<u>กราฟที่ 7</u> แสดงปริมาณเปรียบเทียบการเจริญเพิ่มจำนวนของเม็ดเลือดแดงตัวอ่อนที่เพาะเลี้ยงในอาหาร ชนิดต่าง ๆที่มีขายในปัจจุบันแบบ serum-free โดยเริ่มใช้เซลล์ CD133+ จำนวน 1×10⁵ เซลล์ที่แยก จากเลือดสายสะดือเด็กแรกคลอดและเลี้ยงไว้นาน 15 วัน





Summary Results: Stemline II is excellent for cell multiplication in vitro without serum supplement.

Media	Cell Number (x10 ⁶)						
	Day0	Day5	Day7	Day9	Day11	Day13	Day15
1. Stemline II	0.1	0.9*	3.8*	6.7*	7.6	8	8.2
2. Powerstem	0.1	0.05	0.1	0.05	0	0	0
3. Powerstem Complete	0.1	0.8*	1.8	2	3.6	3.8	4.1
4. Powerstem Complete+G+C	0.1	0.2	1	0.4	0.3	0.3	0.2

5. Powerstem+G+C	0.1	0.2	0.4	0.2	0.4	0.3	0.3
6. Stemspan	0.1	0.1	0.1	0.05	0	0	0
7. Stemspan+G+C	0.1	0.6	2	1.6	2	2.2	1.8

ผลงานวิจัยที่ตีพิมพ์ในวารสารวิชาการระดับนานาชาติ

Shahid Waseem, Michael A. Allen, StefanSchreier, Rachanee Udomsangpetch,
 Sebastian C. Bhakdi*. Antibody-conjugated paramagnetic nanobeads: Kinetics of bead-cell binding. <u>Int. J. Mol. Sci. 2014, 15, 8821-8834</u>; <u>doi:10.3390/ijms15058821</u>

การน้ำผลงานไปใช้ประโยชน์ ยังทำไม่ได้ตามที่วางแผนไว้

การเชื่อมโยงทางวิชาการกับนักวิชาการภายในสถาบันเดียวกัน คือ Dr. Michael A. Allen,
Department of Physics, Faculty of Science, Mahidol University ซึ่งร่วมในการดำเนินงานวิจัยและ
พัฒนา การผลิต Nanomagnetic beads ขึ้นมาใช้งานจนสำเร็จได้ (ดังผลงานตีพิมพ์ดังกล่าวข้างบนนี้)

ปัญหาและอุปสรรค

ความพยายามในการเลี้ยงและเตรียมเม็ดเลือดแดงตัวอ่อนเพื่อเก็บไว้เลี้ยงเชื้อมาลาเรียชนิด P. vivax เราทำการแยกและเลี้ยงเม็ดเลือดแดงตัวอ่อนได้ดี แต่การแยกชนิดเม็ดเลือดแดงตัวอ่อนแต่ละระยะ ออกจากกันนั้นทำได้ยาก เพราะไม่สามารถหา antibody ที่จำเพาะต่อระยะต่างๆของเม็ดเลือดแดงตัว อ่อนได้

การพัฒนาวิธีการแยกเซลล์เม็ดเลือดแดงตัวอ่อนด้วย high-gradient magnetic separation ยังมี ปัญหาด้านคุณภาพการเตรียม nanomagnetic beads ไม่ได้ และเมื่อไม่มี antibody ที่ดีมาประกอบเข้า ไป เราก็ไม่สามารถทำการแยกเม็ดเลือดแดงตัวอ่อนแต่ละระยะออกมาใช้งานการเลี้ยงเชื้อได้ตามที่เสนอ งานไว้

OPEN ACCESS International Journal of Molecular Sciences

ISSN 1422-0067 www.mdpi.com/journal/ijms

Article

Antibody-Conjugated Paramagnetic Nanobeads: Kinetics of Bead-Cell Binding

Shahid Waseem ¹, Michael A. Allen ², Stefan Schreier ³, Rachanee Udomsangpetch ¹ and Sebastian C. Bhakdi ^{1,4,*}

- Department of Pathobiology, Faculty of Science, Mahidol University, Rama 6 Road, Bangkok 10400, Thailand; E-Mails: swaseem92@yahoo.com (S.W.); rachanee.udo@mahidol.ac.th (R.U.)
- Department of Physics, Faculty of Science, Mahidol University, Rama 6 Road, Bangkok 10400, Thailand; E-Mail: maa5652@gmail.com
- Institute for Innovative Learning, Mahidol University, 999 Phuttamonthon 4 Road, Salaya, Nakorn Pathom 73170, Thailand; E-Mail: stefan-schreier@web.de
- ⁴ X-Zell Biotec Co., Ltd., Na-Nakorn Building, 99/349, Moo 2, Chaengwattana Road, Laksi, Bangkok 10210, Thailand
- * Author to whom correspondence should be addressed; E-Mail: sbhakdi@gmail.com; Tel.: +66-2576-1438; Fax: +66-2576-1437.

Received: 3 February 2014; in revised form: 23 April 2014 / Accepted: 24 April 2014 /

Published: 19 May 2014

Abstract: Specific labelling of target cell surfaces using antibody-conjugated paramagnetic nanobeads is essential for efficient magnetic cell separation. However, studies examining parameters determining the kinetics of bead-cell binding are scarce. The present study determines the binding rates for specific and unspecific binding of 150 nm paramagnetic nanobeads to highly purified target and non-target cells. Beads bound to cells were enumerated spectrophotometrically. Results show that the initial bead-cell binding rate and saturation levels depend on initial bead concentration and fit curves of the form $A(1 - \exp(-kt))$. Unspecific binding within conventional experimental time-spans (up to 60 min) was not detectable photometrically. For CD3-positive cells, the probability of specific binding was found to be around 80 times larger than that of unspecific binding.

Keywords: high gradient magnetic separation; bead-cell binding; iron content; paramagnetic nanoparticles; magnetic labeling; cell separation

1. Introduction

Magnetic labelling of cells with paramagnetic nanoparticles is widely used in biomedical sciences. Labelled cells are used in research as well as in clinical diagnostics and therapy, facilitating a range of applications from magnetic cell separation [1] and clinical imaging to targeted drug delivery [2]. The present paper focuses on labelling of cells for magnetic separation of target cells from heterogeneous cell suspensions. For magnetic cell separation in biomedical sciences, high gradient magnetic separation (HGMS) is the most widely used technique, with over 12,000 studies published [3]. Other separation technologies include magnetohydrostatic separation [1,4–7], magnetohydrodynamic separation, and separation using eddy currents [8,9].

In most magnetic cell separation protocols, target cells are labelled with magnetic nanobeads that are conjugated to specific antibodies [10]. The efficiency of magnetic separation is influenced by factors related to the hardware of the magnetic separation system used and factors determined by the quality of the magnetic labelling of cells which depend on the properties or quality of the magnetic nanobeads employed [11]. An ideal magnetic nanobead-based cell labelling system would offer completely specific binding of beads to target cells while completely avoiding binding of beads to non-target cells [12]. To optimize a nanobead-based magnetic separation system, it is therefore crucial to understand the kinetics of specific and unspecific binding of beads to cells.

Previous studies have shown the negative impact of unspecific binding on the downstream recovery rate and purity of the target cells. It was established that optimization of bead concentration can minimize capture of non-target cells during HGMS [13,14].

The present study determines the binding rates for specific and unspecific binding of 150 nm paramagnetic beads to target and non-target cells using highly purified populations of untouched CD3- and CD14-positive cells. These cells often need to be separated in biomedical research. Hence the model is deemed relevant to a large number of biomedical studies. The model allows us to calculate the average number of beads per cell by optimized spectrophotometric measurement of total iron in well-defined populations of labelled target and non-target cells or, in other words, in models of specific and unspecific bead-cell binding.

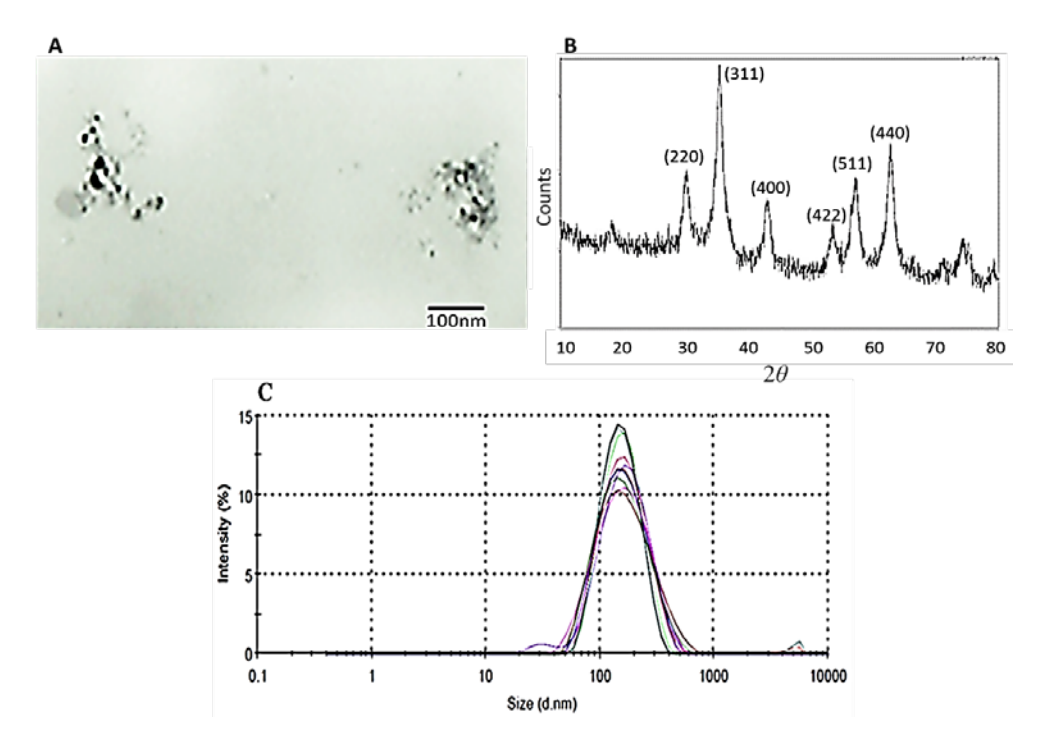
2. Results

2.1. Characterization of Paramagnetic Nanobeads

Manufacturer information described beads as polymer embedded, multi-domain iron oxide cores covalently conjugated to antibodies. Transmission electron microscope (TEM) images showed the iron oxide cores of nanobeads. As expected, the polymer matrix of the nanobeads could not be visualized by TEM. From TEM imaging, the iron oxide cores are estimated to measure 30–50 nm (Figure 1A). X-ray diffraction (XRD) confirmed that the iron oxide crystals consist of pure magnetite (Fe₃O₄) with a characteristic pattern of peaks at angles (2θ) of 30.1, 35.5, 43.1, 53.4, 57.0 and 62.6 which correspond to the Miller indices shown in Figure 1B. Dynamic light scattering (DLS) of antibody-conjugated magnetic nanobeads returned a mean diameter of 158 and 156 nm for anti-CD3 and anti-CD14 beads, respectively, which is consistent with polymer embedding of magnetite crystals as seen in TEM and XRD (Figure 1C). TEM and XRD data are consistent with superparamagnetic iron

oxide (magnetite) nanoparticles as described previously [15,16] and with data provided by the manufacturer. Determination of the antibody concentration of the nanobeads via a UV-Vis spectrophotometer showed $40 \, \mu g$ of antibodies per mg of nanobeads.

Figure 1. Characterization of paramagnetic nanobeads. (**A**) TEM micrograph of antibody-conjugated magnetic nanobeads. The multi-domain iron oxide cores from two nanobeads are visible. Bar size is 100 nm; (**B**) XRD pattern of antibody-conjugated magnetic nanobeads; (**C**) Size distribution of antibody-conjugated magnetic nanobeads is shown by a dynamic light scattering (DLS) graph. Ten replicates, as shown by peaks of different colours, were analysed.



2.2. Enrichment of Untouched CD3- and CD14-Positive Cells by Flow Cytometry

Negative isolation of untouched CD3- or CD14-positive cells was performed as described in the Experimental Section. Over 95% purity was achieved for untouched CD3- or CD14-positive cells in all the experiments. One representative experiment is shown in Figure 2.

2.3. Standard Curve

Standard curves were generated for varying amounts of magnetic nanobeads with or without peripheral blood mononuclear cells (PBMC) using the method described in the Experimental Section. Two million PBMC were used for each data point. A linear relationship was determined between absorbance and number of magnetic beads (Figure 3). The presence of PBMC did not show any significant interference with the linearity of the relationship, especially in the range that proved to be relevant for kinetic experiments (up to 10¹⁰ beads). Calculations for the number of beads per cell for specific or unspecific binding in the proceeding experiments were made according to the standard curve of iron with PBMC (solid line, Figure 3).

Figure 2. Flow cytometric analysis of untouched CD14- and CD3-positive cells separated by buffer optimized high gradient magnetic separation (HGMS) (negative selection). Plots show CD14- and CD3-positive cells before and after magnetic separation. CD14-positive cells were enriched from 17% to 95% and CD3-positive cells from 62% to 96%.

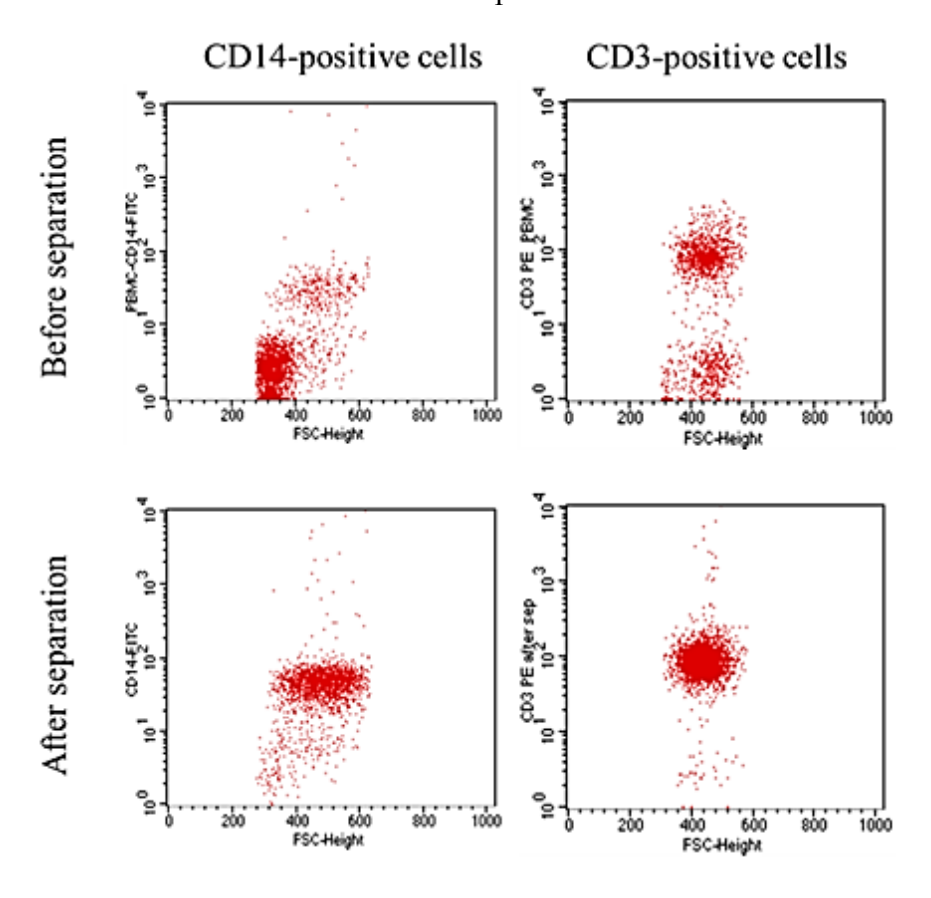
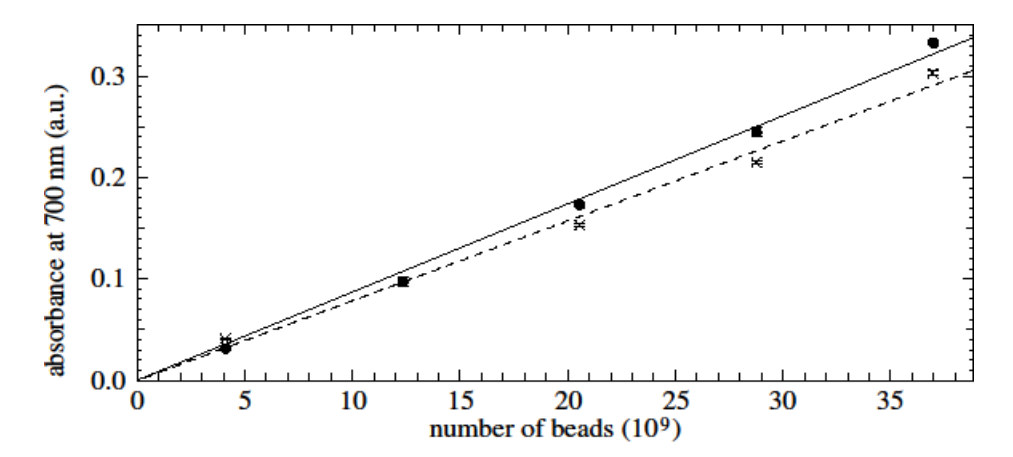


Figure 3. Standard curves for the number of magnetic beads with (solid line, dots) or without peripheral blood mononuclear cells (PBMC) (dashed line, crosses). For both standard curves $R^2 = 0.99$. In this and later figures, data points are the mean of triplicate values. Vertical lines (sometimes smaller than the plotted points) indicate the range of values.



2.4. Quantification of Time-Dependent Binding of Magnetic Nanobeads to Target Cells

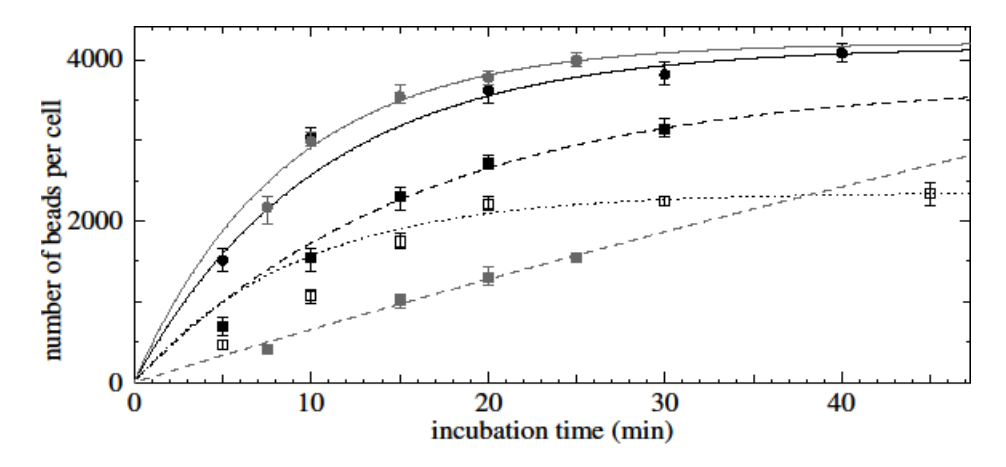
Specific binding assays were performed using anti-CD3 and anti-CD14 conjugated magnetic nanobeads with purified, untouched CD3-positive cells and CD14-positive cells, respectively. To determine the rate of unspecific binding of antibody-coated beads to cells, anti-CD3 labelled beads were incubated with untouched CD14-positive cells and *vice versa*.

Specific and unspecific binding kinetics of nanobeads to target cells were determined at time points varying from 5–45 and 30–300 min, respectively.

2.4.1. Kinetics of Nanobead Binding to Untouched CD3-Positive Cells

The kinetics of specific time-dependent binding of nanobeads to purified untouched CD3-positive cells was determined for different concentrations of nanobeads and target cells. The experiment with the lowest nanobead concentration (8 μ g/100 μ L), where the target cell concentration was maintained at 5 \times 10⁵ cells/100 μ L, did not reach saturation (grey dashed line and square dots, Figure 4). Nanobead concentrations of 16 μ g/100 μ L (dotted line, Figure 4) and 32 μ g/100 μ L (black dashed line, Figure 4) where target cell concentrations were maintained at 1 \times 10⁶/100 and 2 \times 10⁶/100 μ L, respectively, reached saturation after 20 or 30 min of incubation. Interestingly, higher saturation levels were achieved for higher concentrations of nanobeads and higher bead-to-cell ratios.

Figure 4. Time-dependent binding of anti-CD3 conjugated magnetic nanobeads to untouched CD3-positive cells. In this figure and the next, data are fitted to saturation-type curves of the form $A(1 - \exp(-kt))$ where t is the incubation time. Solid black and grey line and round dots: 32 μg beads/100 μL, 10^6 cells/100 μL, $R^2 = 0.95$ and 0.99 (cells from two different donors); black dashed line and square dots: 32 μg beads/100 μL, 2×10^6 cells/100 μL, $R^2 = 0.99$; dotted line and squares: 16 μg beads/100 μL, 10^6 cells/100 μL, 10^6 cel

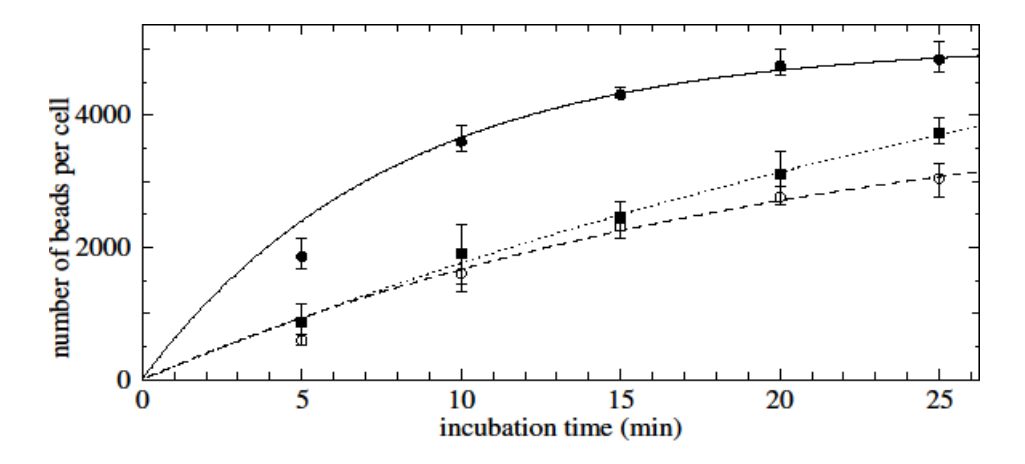


The effect of different blood donors on the kinetics of bead-cell binding was assessed by keeping the concentrations of nanobeads (32 μ g/100 μ L) and untouched CD3-positive cells (1 \times 10⁶/100 μ L) constant. Similar kinetics of bead-cell binding and equal numbers of nanobeads per cell at saturation (~4000 beads per cell) were obtained for the two experiments based on blood samples from two different donors (solid lines, Figure 4).

2.4.2. Kinetics of Nanobead Binding to Untouched CD14-Positive Cells

Kinetics of specific time-dependent binding of nanobeads to highly pure untouched CD14-positive cells were determined for different concentrations of nanobeads keeping the target cell concentrations constant. Saturation levels of around 3500 and 5000 nanobeads per cell were obtained in experiments where the concentration of nanobeads was 16 μ g/100 μ L (dashed and grey lines) and 32 μ g/100 μ L (solid line), respectively. As with the CD3 cells, the saturation levels were higher for the larger bead-to-cell ratio case (Figure 5).

Figure 5. Time-dependent binding of anti-CD14 conjugated magnetic nanobeads to untouched CD14-positive cells. Solid line: 32 µg beads/100 µL, $R^2 = 0.98$; dashed line and circles, dotted line and square dots: 16 µg beads/100 µL, $R^2 = 0.98$ and 0.99. Concentration of target cells: $1 \times 10^6/100$ µL. The experiments are from samples from three different blood donors.



2.4.3. Maximum Bead Saturation of Cells: Specific Binding Assays

To determine the saturation level of specific nanobead-cell binding, saturation experiments were performed by adding an excess of beads, as described in the Experimental Section. It was observed that repeated incubation ("multi-step incubation") of cells with beads increased the number of beads per cell to approximately 10,000. After three steps of bead-cell incubation, the numbers of beads per cell did not increase further. Similar results were found for both anti-CD3 (open circles) and anti-CD14 (solid circles) conjugated magnetic nanobeads (Figure 6).

2.4.4. Unspecific Binding Assays

To examine the rates of unspecific binding of beads to cells, highly purified, untouched populations of CD3 positive cells were incubated with CD14-specific beads and *vice versa*. Around 1000 nanobeads per cell were obtained after 5 h of incubation (Figure 7). The binding rate for unspecific binding was found to be 3.3 beads/cell/min ($R^2 = 0.95$). This scales to 5.0 beads/cell/min for a bead concentration of 10^{12} /mL.

Figure 6. Maximum saturation level for target cells was determined by using multi-step incubation, as described in the Experimental Section. Solid and open circles represent the number of beads per untouched CD14- and CD3-positive cell, respectively.

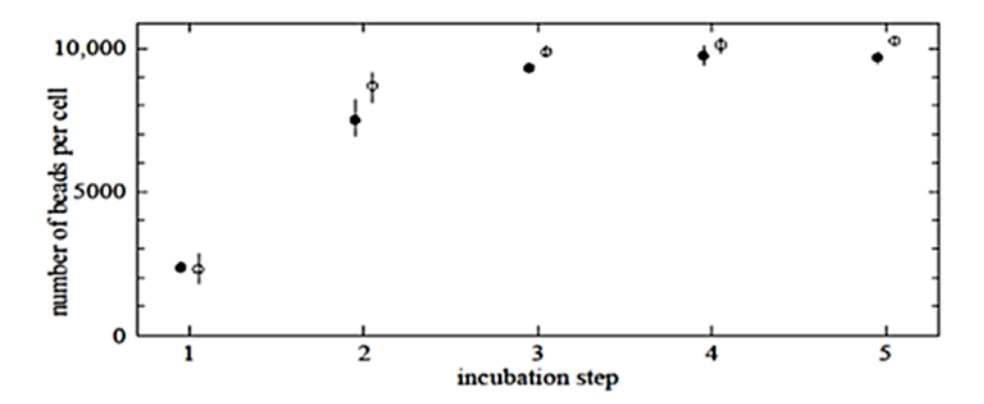
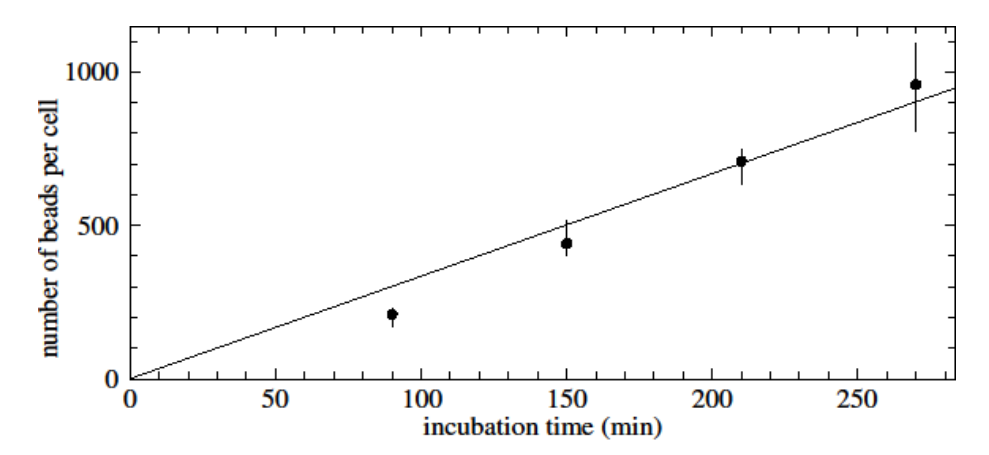


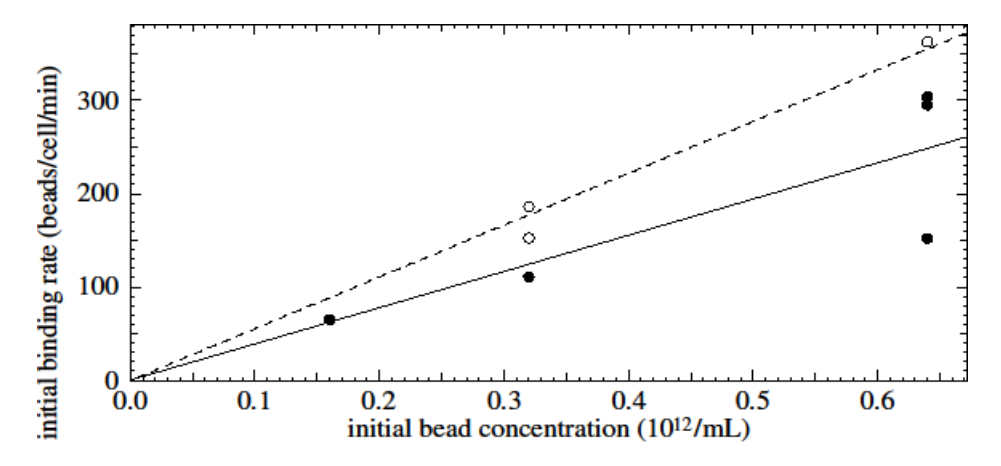
Figure 7. Time-dependent unspecific binding of anti-CD14 conjugated magnetic nanobeads to untouched CD3-positive cells. Concentration of nanobeads: $16 \mu g/100 \mu L$; concentration of target cells: $10^6/100 \mu L$.



2.5. Initial Binding Rate

The initial binding rate was determined by calculating the initial slopes of time-dependent binding curves of untouched CD3- and CD14-positive cells. The initial binding rate (the number of beads binding to a cell per minute) was found to vary linearly with the initial bead concentration (Figure 8). The initial binding rate of beads to untouched CD3-positive cells (solid line, slope 390) is less than that of beads to untouched CD14-positive cells (dashed line, slope 550). Correlation of initial binding rate with initial bead concentration for CD3- and CD14-positive cells was found to be significant with R^2 values of 0.69 and 0.97, respectively. The slope for specific (plus unspecific) binding to CD3 positive cells is 390/5.0 = 80 times larger than the slope would be for unspecific binding to CD3 positive cells. When there is a small amount of unspecific binding, this is roughly the ratio of probabilities for specific and unspecific binding, as is described further in the discussion.

Figure 8. Initial rate of bead-cell binding as a function of initial bead concentration. Solid line and dots: CD3; dashed line and circles: CD14.



3. Discussion

HGMS is the most widely used magnetic cell separation technique for the isolation of magnetically labeled cells from cell suspensions [17]. A cell labelled with magnetic nanobeads will be captured in the HGMS column if the magnetic force acting on the cell is larger than the drag and gravitational forces [8]. In principle, the magnetic force acting on the cell is proportional to its magnetic susceptibility [18], and the magnetic susceptibility of a cell is proportional to the number of magnetic nanobeads bound to the cell.

To optimize any magnetic separation assay it is therefore crucial to understand the kinetics of specific and unspecific bead-cell binding in detail. Previously, unspecific bead-cell binding was examined as a function of bead concentration for different cell types [14]. However, to our knowledge, this is the first time that bead-cell binding kinetics has been examined by direct quantification of magnetic beads on populations of highly purified target and non-target cells. For both specific and unspecific binding assays, sensitive iron detection assays were adopted to determine average numbers of magnetic beads per cell.

CD3-positive cells encompass the entire lymphocyte population present in PBMC, whereas CD14-positive cells are known as monocytes. Both cell types were previously described as expressing 80,000–120,000 receptors per cell [19–24]. Lymphocytes are usually 8–12 µm across, whereas monocytes exist in two well-characterized populations with diameters of 8–10 and 16–20 µm [19–24]. The ratio of the two monocyte populations can be assumed to be 2:1 (smaller:larger) in healthy individuals [19,23–25].

The antibody-conjugated magnetic nanobeads employed in the study were found to be 150–160 nm in diameter with magnetite crystal cores of 30–50 nm, as determined by DLS and TEM images.

Results showed that the initial binding rate of beads to cells is proportional to the initial bead concentration employed during bead-cell incubation. Experimental data of time-dependent assays showed saturation-type curves for all cell- and bead-type combinations.

We assume that the rate at which beads bind to cells (db/dt) where b is the number of beads per cell) is proportional to the concentration of viable beads in solution (which is $n_0 - n_c b$ where n_0 is the initial bead concentration and n_c is the concentration of cells) and to the remaining area on the cell that can be

occupied by beads (which is proportional to $b_{\text{max}} - b$ where b_{max} is the maximum possible number of beads per cell). Hence $db/dt = C(n_0 - n_c b)(b_{\text{max}} - b)$ where C is the constant of proportionality which is itself proportional to the probability of binding. The solutions to this equation are saturation type curves which have an initial value of db/dt (the initial binding rate when b is still small) of Cn_0b_{max} . One would therefore expect that the initial binding rate is proportional to the bead concentration.

Later during the course of bead-cell binding, the value of b levels off at b_{max} when $n_0 > n_c b_{\text{max}}$ (i.e., when there are enough beads in solution to saturate the cells) and at n_0/n_c when $n_0 < n_c b_{\text{max}}$ which is when there are not enough beads to saturate the cells. For the cases $n_0 > n_c b_{\text{max}}$ and $n_0 < n_c b_{\text{max}}$, these saturation curves are approximately of the form $A(1 - \exp(-kt))$. Indeed, as shown in the results, fitting saturation-type curves of the form $A(1 - \exp(-kt))$ to the experimental data returned significant R^2 values, corroborating the assumption of classical, concentration-dependent saturation-type kinetics based on the theory outlined here.

To determine the maximum possible number of beads per cell, multi-step incubation experiments were performed. These gave higher saturation levels than single-step incubation experiments with increased bead concentrations (data not shown). Regarding the cells as spheres, the cell surface area is $4\pi R^2$ where $R \sim 5$ µm is the radius of a cell, and treating the attached nanobeads conjugated to antibodies as discs of radius $r \sim 80$ nm, it would appear that the maximum number of beads on a cell surface would be $4\pi R^2 f/(\pi r^2)$ where f is the maximum fraction of the cell surface area that can be covered by beads without overlap. Assuming that $f = \pi/\sqrt{12} = 0.91$, the value for close packing of discs on a plane, gives in the order of 14,000 beads per cell. Saturation levels in multi-step incubation experiments reached approximately 10,000 beads per cell, which seems consistent with the above calculation allowing for the fact that there is a distribution of cell and bead sizes. This also corresponds with previous studies that demonstrated steric saturation of cell surfaces with nanobeads [13].

Perhaps the more interesting observation is that experiments without multi-step binding protocol show slowing of bead-binding rates and apparent saturation at much lower levels of beads per cell. A possible explanation is that the quality of beads is probably not consistent even within the same batch. Firstly, during production of nanometre-sized particles, the number of functional groups essential for antibody conjugation is difficult to control per particle, as assays of individual particles are not yet possible. Secondly, after antibody-bead conjugation, orientation and functionality of antibodies is also random to a certain extent, which further increases variability between beads. Hence it can be assumed that during the incubation of a seemingly homogenous population of nanobeads with cells, high-quality (i.e., highly reactive) beads are depleted first, and leftover lower quality beads contribute to a progressively slowing bead-cell binding rate, which would result in the case of $n_0 < n_c b_{max}$, even if only looking at bead numbers would lead to the initial assumption $n_0 > n_c b_{max}$.

This unknown distribution could partly be characterized by a combination of the change of the binding rate over time, the ratio of the maximum saturation levels in multi-step incubation experiments, and saturation levels observed in kinetic, single-incubation experiments. Elucidating further parameters to characterize the distribution in detail certainly warrants further research, since its better understanding harbours the potential to advance validation of assays involving binding of nanobeads to cells.

4. Experimental Section

4.1. Preparation of Mononuclear Cells

Whole blood was obtained from healthy donors after informed consent. PBMC were prepared by density gradient centrifugation as described previously [26]. Briefly, whole blood was mixed with an equal volume of PBS (Biochrom, Berlin, Germany). Subsequently, blood was pipetted on top of an equal volume of Lymphoprep (Axis-Shield PoC AS, Oslo, Norway) and centrifuged at $800 \times g$ for 20 min at 20 °C. PBMC were collected at the interface and then washed twice with PBS at $300 \times g$ for 10 min at 20 °C. Cell concentration was determined by haemocytometer (Boeco, Hamburg, Germany) using the trypan blue (Gibco, Life Technologies, Stockholm, Sweden) exclusion method.

4.2. Characterization of Paramagnetic Nanobeads

The 150 nm HMX anti-human anti-CD3, anti-CD14, and anti-biotin magnetic beads were from X-Zell Biotec, Bangkok, Thailand. According to the manufacturer, antibodies were conjugated to carboxyl-functionalized polysaccharide beads containing a multi-domain magnetite core by carbodiimide chemistry. The size distribution, morphology, and crystallinity of the nanobeads were determined by dynamic light scattering (DLS), transmission electron microscopy (TEM), and X-ray diffraction (XRD), respectively. For the DLS, the bead suspension was analysed in a Zetasizer (Malvern Instruments Ltd., Worcestershire, UK). For the TEM, an aqueous solution of the nanobeads was dispersed on a copper grid, dried under vacuum, and micrographs were recorded using a Hitachi-600 electron microscope at 80 kV. The XRD experiment was performed using a Rigaku (TTRAX III) X-ray diffractometer with fixed monochromater at a wavelength and speed of 0.1542 nm and 3°/min, respectively.

The amount of antibody on the beads was determined by a Bradford assay. Briefly, antibody-conjugated nanobeads were placed in Bradford solution for 60 min and the protein concentration was determined using a NanoDrop spectrophotometer ND-1000 (Thermo Fisher Scientific, Waltham, MA, USA) at 595 nm.

4.3. Isolation of Untouched CD3- and CD14-Positive Cells

4.3.1. Magnetic Labeling

Untouched CD3- or CD14-positive cells were isolated from PBMC using buffer-optimized HGMS, anti-biotin magnetic beads, and a biotinylated antibody cocktail. The cocktail contained anti-CD14, -CD16, -CD19, -CD123, -CD235a for untouched CD3-positive cells, and anti-CD3, -CD7 -CD16, -CD19, -CD56 -CD123, -CD235a for untouched CD14-positive cells. All reagents were from X-Zell Biotec, Bangkok, Thailand. Briefly, PBMC were resuspended in HGMS buffer (3% BSA/PBS, pH 7.4) and incubated with human TruStain FcX (BioLegend, San Diego, CA, USA) (5 μL per 2 × 10⁶ cells) for 5–10 min at 4 °C to block Fc receptors. 10 μL of biotinylated antibody cocktail (for untouched CD3- or CD14-positive cells) was added and incubated for 10 min at 4 °C. Finally, anti-biotin magnetic beads were mixed and incubated for 15 min at 4 °C. The incubation mixture was shaken every 5 min by finger tapping and finally washed (300× g at 4 °C for 10 min).

The incubation volume was maintained at 250 μ L. Fresh, filtered, cold buffer (3% BSA/PBS, pH 7.4) was used in the assay.

4.3.2. Magnetic Isolation of Untouched CD3- and CD14-Positive Cells

Magnetically labeled PBMC were resuspended in HGMS buffer (3% BSA/PBS, pH 7.4) (500 μ L/10⁷ cells) and subjected to magnetic separation as described previously [27]. Briefly, the HGMS column was filled with HGMS buffer. Air bubbles were removed by gentle finger tapping. The HGMS column was placed inside an HGMS magnet 5 min before loading the sample. The HGMS column was connected to a 26G/½-inch needle via a stopcock. Magnetically labelled PBMC were loaded onto the column while the stopcock was opened. The column was washed with 8–10 mL buffer (0.5% BSA/PBS, pH 7.4) at a flow rate of 0.33 mL/min. The target cells (untouched CD3- or CD14-positive cells) were allowed to flow through. The flow-through was centrifuged and target cells were pelleted at 300× g for 10 min at 4 °C. The concentration of the target cells was measured using a haemocytometer by the trypan blue exclusion method. Fresh, filtered, cold buffers (3% BSA/PBS or 0.5% BSA/PBS; pH 7.4) were used in the assay. The HGMS columns and magnet were from X-Zell Biotec, Bangkok, Thailand.

4.4. Flow Cytometry

The purity of the untouched CD3- or CD14-positive cells was determined using a FACScan flow cytometer (BD, Erembodegem, Belgium). Cells were labelled with anti-CD3 or anti-CD14 antibodies (Exbio, Prague, Czech Republic) conjugated with phycoerythrin (R-PE) or fluorescein (FITC) (Innova Biosciences, Cambridge, UK). Cells were analysed before and after magnetic separation to confirm enrichment. 10,000 events were acquired from each sample. Unstained untouched CD3- or CD14-positive cells (after magnetic separation) were used as a negative control.

4.5. Quantification of the Average Number of Beads per Cell

4.5.1. Standard Curve

Non-coated 150 nm HMX beads were used in the assay (X-Zell Biotec, Bangkok, Thailand). The bead diameter was 150 nm and the bead concentration was 4.11×10^9 beads/µg. The average number of beads per cell was quantified by creating standard curves of known numbers of beads using a photometric iron quantification assay as described previously [4].

Briefly, magnetic beads in distilled water containing 1, 3, 5, 7 and 9 μ g beads were placed in 1.5 mL centrifuge tubes (SPL Lifesciences, Gyeonggi-Do, Korea) and PBMC were added as indicated. The bead-cell mixture was dried at 70 °C overnight. After the liquid evaporated completely, dried magnetic beads were soaked in 100 μ L HCl (5M) (Thermo Fisher Scientific, Waltham, MA, USA), vortexed, and incubated at 60 °C for 4 h. Caps of the tubes were kept on to avoid evaporation. After incubation, two-fold dilution was made with freshly prepared 5% potassium hexacyanoferrate (II) (Fluka AG, Buchs, Switzerland) and the tubes were incubated for a further 35 min at room temperature in the dark. The mixture was centrifuged at $9700 \times g$ for 10 min. The iron content was quantified by measuring the absorption in a NanoDrop spectrophotometer ND-1000 (Thermo Fisher Scientific, Waltham, MA, USA) at 700 nm. Triplicate samples were analysed.

4.5.2. Magnetic Beads per Cell

Kinetics of Bead-Cell Binding

To determine the number of magnetic beads on untouched CD3- or CD14-positive cells, the untouched CD3- or CD14-positive cells (2×10^6 cells, and in one case, 5×10^5 cells) were incubated with anti-CD3 or anti-CD14 magnetic beads (X-Zell Biotec, Bangkok, Thailand), respectively, in 5% BSA/PBS at 4 °C for 5–45 min. The incubation volume was maintained at 200 μ L. Each cell suspension was agitated every 5 or 10 min by gentle tapping.

At the end of the incubation period, the cell suspension was diluted up to 10 mL and washed twice at $300 \times g$ for 10 min at 4 °C to wash away unbound magnetic beads. The cells were then pelleted, dried at 70 °C overnight, and the average number of beads was obtained by determining the total iron content as described in 4.5.1.

Maximum Bead Saturation: Specific Binding Assay

To determine the maximum saturation level per target cell, the following protocol was established. Saturation curves for specific binding for highly pure untouched CD3- or CD14-positive cells were determined by incubating target cells with anti-CD3 or anti-CD14 magnetic beads, respectively. Five sample tubes (1, 2, 3, 4 and 5) were prepared and subjected to one, two, three, four, and five incubation steps, respectively. The time for each incubation step was set at 30 min. The total amount of magnetic beads used for one, two, three, four, and five incubation steps was, respectively, 16, 64, 80, 96 and 112 μ g per 1 \times 10⁶ target cells per 100 μ L. After the first incubation step, target cells were pelleted and resuspended in buffer, and the magnetic beads were mixed and incubated for the next 30 min at 4 °C. The incubation mixture was agitated gently every 10 min. All remaining incubation steps were performed in the same way.

Maximum Bead Saturation: Unspecific Binding Assay

To investigate the maximum saturation level per non-target cell (unspecific binding), anti-CD3 magnetic beads were incubated with untouched CD14-positive cells (2×10^6 cells) and *vice versa*. The iron content was determined and the protocol was followed as described above.

5. Conclusions

The results demonstrated that the initial binding rate of magnetic nanobeads to cells is proportional to the initial bead concentration. The measured numbers of bound beads per cell as a function of time fit saturation-type curves of the form $A(1 - \exp(-kt))$, and levels of binding after single-step incubation experiments are significantly lower than the levels achieved in multi-step incubation assays, which might be attributed to a previously unknown bead quality distribution. Our results show that the probability that a bead binds specifically is around 80 times that for unspecific binding. This explains our observation that unspecific binding within conventional experimental time-spans (up to 60 min) was not detectable photometrically.

Acknowledgments

This study was supported by the Thailand Research Fund (BRG53_0052) and the Faculty of Graduate Studies (Research Assistantship Grant), Mahidol University, Bangkok, Thailand. We thank Prukswan Chetanachan, Electron Microscopy Unit, Department of Medical Sciences, National Institute of Health, for providing the TEM micrographs.

Conflicts of Interest

S.C.B. is shareholder of X-Zell Biotec (Bangkok, Thailand). The other authors declare no conflict of interest.

References

- 1. Miltenyi, S.; Muller, W.; Weichel, W.; Radbruch, A. High gradient magnetic cell separation with MACS. *Cytometry* **1990**, *11*, 231–238.
- 2. Wang, Z.; Cuschieri, A. Tumour cell labeling by magnetic nanoparticles with determination of intracellular iron content and spatial distribution of the intracellular iron. *Int. J. Mol. Sci.* **2013**, *14*, 9111–9125.
- 3. Grützkau, A.; Radbruch, A. Small but mighty: How the MACS-technology based on nanosized superparamagnetic particles has helped to analyze the immune system within the last 20 years. *Cytometry A* **2010**, *77*, 643–647.
- 4. Rad, A.M.; Janic, B.; Iskander, A.; Soltanian-Zadeh, H.; Arbab, A.S. Measurement of quantity of iron in magnetically labeled cells: Comparison among different UV/Vis spectrometric methods. *Biotechniques* **2007**, *43*, 627–636.
- 5. Sundstrom, J.B.; Mao, H.; Santoianni, R.; Villinger, F.; Little, D.M.; Huynh, T.T.; Mayne, A.E.; Hao, E.; Ansari, A.A. Magnetic resonance imaging of activated proliferating *Rhesus macaque* T cells labeled with superparamagnetic monocrystalline iron oxide nanoparticles. *J. Acquir. Immune Defic. Syndr.* **2004**, *35*, 9–21.
- 6. Šafařík, I.; Šafaříková, M. Use of magnetic techniques for the isolation of cells. *J. Chromatogr. B* **1999**, 722, 33–53.
- 7. Pankhurst, Q.A.; Connolly, J.; Jones, S.; Dobson, J. Applications of magnetic nanoparticles in biomedicine. *J. Phys. D* **2003**, *36*, R167–R181.
- 8. Iacob, G.; Ciochina, A.D.; Bredetean, O. High gradient magnetic separation ordered matrices. *Eur. Cells Mater.* **2002**, *3*, 167–169.
- 9. Oberteuffer, J. High gradient magnetic separation. *IEEE Trans. Magn.* **1973**, *9*, 303–306.
- 10. Molday, R.S.; Mackenzie, D. Immunospecific ferromagnetic iron-dextran reagents for the labeling and magnetic separation of cells. *J. Immunol. Methods* **1982**, *52*, 353–367.
- 11. Kim, Y.G.; Song, J.B.; Yang, D.G.; Lee, J.S.; Park, Y.J.; Kang, D.H.; Lee, H.G. Effects of filter shapes on the capture efficiency of a superconducting high-gradient magnetic separation system. *Supercond. Sci. Technol.* **2013**, *26*, 085002.
- 12. Foddai, A.; Elliott, C.T.; Grant, I.R. Maximizing capture efficiency and specificity of magnetic separation for *Mycobacterium avium* subsp. Paratuberculosis cells. *Appl. Environ. Microbiol.* **2010**, *76*, 7550–7558.

- 13. Zhang, H.; Williams, P.S.; Zborowski, M.; Chalmers, J.J. Binding affinities/avidities of antibody-antigen interactions: Quantification and scale-up implications. *Biotechnol. Bioeng.* **2006**, *95*, 812–829.
- 14. Chalmers, J.; Xiong, Y.; Jin, X.; Shao, M.; Tong, X.; Farag, S.; Zborowski, M. Quantification of non-specific binding of magnetic micro-and nanoparticles using cell tracking velocimetry: Implication for magnetic cell separation and detection. *Biotechnol. Bioeng.* **2010**, *105*, 1078–1093.
- 15. Butler, R.F.; Banerjee, S.K. Theoretical single-domain grain size range in magnetite and titanomagnetite. *J. Geophys. Res.* **1975**, *80*, 4049–4058.
- 16. Baumgartner, J.; Bertinetti, L.; Widdrat, M.; Hirt, A.M.; Faivre, D. Formation of magnetite nanoparticles at low temperature: from superparamagnetic to stable single domain particles. *PLoS One* **2013**, *8*, e57070.
- 17. McCloskey, K.E.; Chalmers, J.J.; Zborowski, M. Magnetophoretic mobilities correlate to antibody binding capacities. *Cytometry* **2000**, *40*, 307–315.
- 18. Han, K.-H.; Frazier, A.B. Paramagnetic capture mode magnetophoretic microseparator for high efficiency blood cell separations. *Lab Chip* **2006**, *6*, 265–273.
- 19. Ginaldi, L.; Matutes, E.; Farahat, N.; de Martinis, M.; Morilla, R.; Catovsky, D. Differential expression of CD3 and CD7 in T-cell malignancies: A quantitative study by flow cytometry. *Br. J. Haematol.* **1996**, *93*, 921–927.
- 20. Kristenson, A. The variations in size (the lymphocyte profile) of the lymphocytes circulating in the blood in some normal and pathological conditions. *Acta Medica Scand.* **1949**, *133*, 157–161.
- 21. Muratore, F.; Mannino, N.; Vulpis, N. Variations of the size of fresh lymphocytes in normal and pathological conditions. *Boll. Soc. Ital. Biol. Sper.* **1950**, *26*, 1187–1189.
- 22. Couturier, C.; Haeffner-Cavaillon, N.; Caroff, M.; Kazatchkine, M.D. Binding sites for endotoxins (lipopolysaccharides) on human monocytes. *J. Immunol.* **1991**, *147*, 1899–1904.
- 23. Passlick, B.; Flieger, D.; Ziegler-Heitbrock, H.W. Identification and characterization of a novel monocyte subpopulation in human peripheral blood. *Blood* **1989**, *74*, 2527–2534.
- 24. Wang, S.Y.; Mak, K.L.; Chen, L.Y.; Chou, M.P.; Ho, C.K. Heterogeneity of human blood monocyte: Two subpopulations with different sizes, phenotypes and functions. *Immunology* **1992**, *77*, 298–303.
- 25. Ziegler-Heitbrock, H.W.; Strobel, M.; Kieper, D.; Fingerle, G.; Schlunck, T.; Petersmann, I.; Ellwart, J.; Blumenstein, M.; Haas, J.G. Differential expression of cytokines in human blood monocyte subpopulations. *Blood* **1992**, *79*, 503–511.
- 26. Panichakul, T.; Sattabongkot, J.; Chotivanich, K.; Sirichaisinthop, J.; Cui, L.; Udomsangpetch, R. Production of erythropoietic cells *in vitro* for continuous culture of *Plasmodium vivax*. *Int. J. Parasitol.* **2007**, *37*, 1551–1557.
- 27. Bhakdi, S.; Ottinger, A.; Somsri, S.; Sratongno, P.; Pannadaporn, P.; Chimma, P.; Malasit, P.; Pattanapanyasat, K.; Neumann, H. Optimized high gradient magnetic separation for isolation of *Plasmodium*-infected red blood cells. *Malar. J.* **2010**, *9*, 1–9.
- © 2014 by the authors; licensee MDPI, Basel, Switzerland. This article is an open access article distributed under the terms and conditions of the Creative Commons Attribution license (http://creativecommons.org/licenses/by/3.0/).



Sebastian Punyaratabandhu Bhakdi sbhakdi@gmail.com

Your Submission

Samuel Bader < jmmm@anl.gov>

21. August 2014 um 02:28

An: sbhakdi@gmail.com

Ms. Ref. No.: MAGMA-D-13-00540

Title: Buffer-optimized high gradient magnetic separation: target cell capture efficiency is predicted by linear bead-capture theory

Journal of Magnetism and Magnetic Materials

Dear Dr.Med. Sebastian Chakrit Bhakdi,

I apologize for the serious delay in the review process of your manuscript. We have been unable to find a reviewer to provide a review of your manuscript. Therefore we are returning it to you so that you can submit to a journal in your reference list where it will reach an appropriate audience.

Thank you for giving us the opportunity to consider your work.

Yours sincerely,

Samuel D. Bader Editor Journal of Magnetism and Magnetic Materials

For further assistance, please visit our customer support site at http://help.elsevier.com/app/answers/list/p/7923. Here you can search for solutions on a range of topics, find answers to frequently asked questions and learn more about EES via interactive tutorials. You will also find our 24/7 support contact details should you need any further assistance from one of our customer support representatives.

Elsevier Editorial System(tm) for Journal of Magnetism and Magnetic Materials Manuscript Draft

Manuscript Number: MAGMA-D-13-00540

Title: Buffer-optimized high gradient magnetic separation: target cell capture efficiency is predicted by

linear bead-capture theory

Article Type: Regular Submission

Keywords: high gradient magnetic separation, linear bead-capture theory, capture efficiency, CD3-

positive cells,

CD14-positive cells, functional assays

Corresponding Author: Dr.Med. Sebastian Chakrit Bhakdi, MD

Corresponding Author's Institution: Faculty of Science, Mahidol University

First Author: Shahid Waseem, MSc

Order of Authors: Shahid Waseem, MSc; Michael A Allen, PhD; Stefan Schreier, PhD; Rachanee

Udomsangpetch, PhD; sebastian C bhakdi

Abstract: High gradient magnetic separation (HGMS) is the most commonly used magnetic cell separation technique in biomedical science. However, parameters determining target cell capture efficiencies in HGMS still lack systematic characterization. Low target cell capture efficiencies frequently lead to loss of information and resources. The present study develops linear bead-capture theory to predict capture efficiencies in HGMS. The theory is tested on a generic HGMS system by combining CD3- and CD14-positive cells with antibody-labeled, paramagnetic beads of different diameters. To rule out adverse biological effects of adjusting bead diameters, it is further demonstrated that physiological key functions of cells are not affected by respective experimental conditions.

Dear Editor,

Please find enclosed our manuscript

Buffer-optimized high gradient magnetic separation: target cell capture efficiency is predicted by linear bead-capture theory

to be considered for publication in the Journal of magnetism and magnetic materials.

High gradient magnetic separation is the most widely used magnetic cell separation method in biomedical science. While separation purities were optimized with the introduction of the commercial MACS system over 20 years ago, parameters determining capture efficiencies are still not well understood.

The present manuscript develops and tests linear bead-capture theory to better predict capture efficiencies. The theory may serve as a basis to develop improved protocols for HGMS isolation of certain sub-groups of cells, of which inconsistent capture efficiencies were reported previously, for example certain groups of stem cells.

I am looking forward to hearing from you,

Yours sincerely,

Sebastian C Bhakdi, MD Corresponding author

Email: sbhakdi@gmail.com

*Highlights (for review)

Highlights

- ▲ Linear bead-capture theory for optimization of target-cell capture efficiencies in high gradient magnetic separation is developed
- ▲ The theory predicts cell capture efficiencies in generic buffer-optimized high gradient magnetic separation
- Adverse biological effects of different paramagnetic bead diameters are excluded by functional assays

Buffer-optimized high gradient magnetic separation: target cell capture efficiency is predicted by linear bead-capture theory

Shahid Waseem^a, Michael A. Allen^b, Stefan Schreier^c, Rachanee Udomsangpetch^a, Sebastian C. Bhakdi^{a,d,*}

^aDepartment of Pathobiology, Faculty of Science, Mahidol University, Rama 6 Road, Bangkok 10400, Thailand
 ^bPhysics Department, Mahidol University, Rama 6 Road, Bangkok 10400, Thailand
 ^cInstitute for Innovative Learning, Mahidol University, 999 Phuttamonthon 4 Road, Salaya, Nakorn Pathom 73170, Thailand

Abstract

High gradient magnetic separation (HGMS) is the most commonly used magnetic cell separation technique in biomedical science. However, parameters determining target cell capture efficiencies in HGMS still lack systematic characterization. Low target cell capture efficiencies frequently lead to loss of information and resources. The present study develops linear bead-capture theory to predict capture efficiencies in HGMS. The theory is tested on a generic HGMS system by combining CD3- and CD14-positive cells with antibody-labeled, paramagnetic beads of different diameters. To rule out adverse biological effects of adjusting bead diameters, it is further demonstrated that physiological key functions of cells are not affected by respective experimental conditions.

Keywords: high gradient magnetic separation, capture efficiency, recovery rate, CD3-positive cells, CD14-positive cells

1. Introduction

10

15

Over the past three decades, magnetic cell separation has been established as an important tool in biomedical research. To isolate a particular subgroup of cells from a heterogeneous cell suspension, target cells are labelled with paramagnetic beads that are attached to specific antibodies. Commercially available techniques include conventional magnetic separation (Dynal, Invitrogen, Carlsbad, USA), the technically more sophisticated quadrupole separation (EasySep, Stem Cell techniques, Vancouver), and high gradient magnetic separation (MACS, Miltenyi Biotec, Germany). Bead sizes range from several micrometres down to tens of nanometres, and the choice of bead size plays an important role as to which magnetic separation technique can be employed. Micrometre-sized beads can be separated by conventional magnets but usually require removal after separation since they interfere with flow cytometric or light microscopic readout systems. It has also been reported that these larger bead sizes can lead to polyvalent binding, or in other words, cross linking of receptors which leads to activation of sensitive cells and/or to endocytosis of beads [1]. Currently, nanosized beads are therefore preferred for most applications. However, because of the significantly lower amounts of paramagnetic material attached to each cell, they require one of the two more sophisticated magnetic separation techniques.

The most widespread technique for separation of very weakly paramagnetic bodies is high gradient magnetic separation (HGMS). In HGMS, a matrix of thin filaments or spheres of ferromagnetic material is placed in a strong homogeneous magnetic field. With this technique, magnetic field gradients of up to 100 T/cm can be created at the surface of the matrix [2]. Early work on generic HGMS systems [3, 4]

Email address: sbhakdi@gmail.com (Sebastian C. Bhakdi)

 $[^]dX\text{-}Zell\ Biotech\ Co.,\ Ltd.,\ Na\text{-}Nakorn\ Building,\ 99/349,\ Moo\ 2,\ Chaengwattana\ Road,\ Laksi,\ Bangkok\ 10210,\ Thailand\ South Co.,\ S$

^{*}Corresponding author

eventually led to the development of the MACS HGMS system [5]. Today, the MACS system is still the only viable commercially available HGMS technique in cell biology, with over 12 000 studies published during the past two decades [6].

The MACS system relies on HGMS in combination with 20–100 nm diameter paramagnetic beads. However, while separation purities are generally reported to be acceptable, capture efficiencies ($E_{\rm t} = [{\rm target}$ cells isolated]/[total target cell loaded]) are not always consistent between different researchers and different target cell types. In many cases this leads to loss of information and resources [7].

The present study develops linear bead-capture theory to describe practical predictive parameters for $E_{\rm t}$ in HGMS. The theory is tested by labelling two different cell types with commercially available magnetic beads of 50 nm and 100 nm diameter. Buffer-optimized HGMS serves as a readout system for $E_{\rm t}$, as described previously [8], and functional assays demonstrate viability of isolated cells.

2. Theory

20

25

30

35

40

45

50

55

60

2.1. Capture of beads by cells

We treat the cells and beads as spheres. The mean speed of a body in equilibrium with its surroundings is inversely proportional to the square root of its mass. The smallest cell (7 μ m diameter) has a mass 70^3 times that of the largest bead used (0.1 μ m diameter), assuming both have the same density. Hence the unattached beads have an average speed which is at least $\sqrt{70^3} \sim 600$ times that of the cells. We therefore regard the cells as being stationary and subject to a flux of beads κn where n is the number density of the unattached viable beads and κ is a constant [9]. Let B(t) and W(t) denote, respectively, the total numbers of beads attached to antigens on the target cells and bound non-specifically (either to target cells or to other cells) at time t. The beads are added at t=0 and so B(0)=W(0)=0. The number of unattached viable beads, N(t) = N(0) - B(t) - W(t), and n = N/V where V is the volume of the suspension. Let $A_{\rm sb}$ be the maximum possible total cell surface area taken up by specifically bound beads. If $r_{\rm b}$ is the radius of a bead then $A_{\rm sb} = \alpha_{\rm t} N_{\rm c} b_{\rm max} \pi r_{\rm b}^2$ where $N_{\rm c}$ is the number of cells, $\alpha_{\rm t}$ is the fraction of cells which are target cells, and b_{max} is the maximum number of beads that can be bound to antigens on a target cell and is given by

$$b_{\rm max} = \min(a, \varphi d_{\rm t}^2/r_{\rm b}^2)$$

where a is the number of antigens per target cell and φ is the fraction of the cell surface area that can be covered by beads. We assume that $\varphi = \pi/\sqrt{12} = 0.9069$, the value for close packing of discs on a plane. The total surface area available for non-specific binding before any beads are present on all the cells is given by

$$A_{\rm nsb} = \pi \varphi N_{\rm c} \sum_i \alpha_i d_i^2 - A_{\rm sb}$$

where d_i and α_i are the root mean squared diameter of and proportion of cells that are cell type i.

To avoid making the model too detailed, we make the following assumptions: (i) the antigens are uniformly distributed on the target cells (ii) beads only attach to areas not already occupied by a bead (iii) a bead has a chance of attaching to an antigen if the point at which the bead initially touches the cell is less than $r_{\rm b}$ from the antigen (iv) non-specific binding never approaches saturation (i.e., $W\pi r_{\rm b}^2 \ll A_{\rm nsb}$). Then we have

$$\frac{\mathrm{d}B}{\mathrm{d}t} = \beta \kappa n (A_{\rm sb} - B\pi r_{\rm b}^2),\tag{1}$$

$$\frac{\mathrm{d}B}{\mathrm{d}t} = \beta \kappa n (A_{\rm sb} - B\pi r_{\rm b}^2), \tag{1}$$

$$\frac{\mathrm{d}W}{\mathrm{d}t} = \gamma \kappa n (A_{\rm nsb} - W\pi r_{\rm b}^2) \tag{2}$$

where β and γ are the fraction of times that a viable bead sticks when colliding with, respectively, an antigen or another part of the cell surface. Dividing (1) and (2) by $\alpha_t N_c$ and N_c , respectively, gives

$$\frac{\mathrm{d}b}{\mathrm{d}t} = \beta \pi r_{\mathrm{b}}^{2} \kappa (n_{0} - \alpha_{\mathrm{t}} n_{\mathrm{c}} b - n_{\mathrm{c}} w) (b_{\mathrm{max}} - b),$$

$$\frac{\mathrm{d}w}{\mathrm{d}t} = \gamma \pi r_{\mathrm{b}}^{2} \kappa (n_{0} - \alpha_{\mathrm{t}} n_{\mathrm{c}} b - n_{\mathrm{c}} w) (w_{\mathrm{max}} - w)$$
(4)

$$\frac{\mathrm{d}w}{\mathrm{d}t} = \gamma \pi r_{\mathrm{b}}^2 \kappa (n_0 - \alpha_{\mathrm{t}} n_{\mathrm{c}} b - n_{\mathrm{c}} w) (w_{\mathrm{max}} - w) \tag{4}$$

where b is the mean number of beads attached to antigens on a target cell, w is the mean number of non-specifically bound beads on any cell, n_0 is the initial number density of viable unattached beads, and

$$w_{\rm max} \equiv \frac{\varphi}{r_{\rm b}^2} \sum_i \alpha_i d_i^2 - \alpha_{\rm t} b_{\rm max}.$$

The coupled nonlinear equations (3) and (4) cannot be solved analytically. However, the behaviour of b and w is straightforward; both increase monotonically from zero and will saturate as either factor in brackets on the right-hand sides approaches zero. When $b \ll b_{\text{max}}$, $w \ll w_{\text{max}}$, and $\alpha_t n_c b + n_c w \ll n_0$ the right-hand sides are approximately constant and are both proportional to n_0 . We refer to this case as the linear regime.

The number of beads attached to target cells is $B + (A_{\rm nsbt}/A_{\rm nsb})W$ where the total area not occupied by antigens on the target cells, $A_{\rm nsbt} = \pi \alpha_{\rm t} N_{\rm c} \varphi d_{\rm t}^2 - A_{\rm sb}$. Hence $c_{\rm t}$, the mean number of beads attached to a target cell, is given by

$$c_{\rm t} = b + \left(\frac{\varphi d_{\rm t}^2 - b_{\rm max} r_{\rm b}^2}{w_{\rm max} r_{\rm b}^2}\right) w. \tag{5}$$

In the linear regime c_t is therefore also proportional to n_0 .

2.2. HGMS capture efficiency

65

70

75

80

85

90

95

According to [10], the capture efficiency for a cell of type i (i.e., [the number of cells of type i captured]/[the number of cells of type i that enter column]) is given by

$$E_i = 1 - \exp\left(-\frac{\langle h \rangle d_i^2 F L \chi_i M B_0}{36\pi \eta r_{\text{pbp}}^2 v_f}\right)$$
 (6)

where $\langle h \rangle$ is the geometric factor (which is 4/3 for a random filter), F is the filter filling factor (0.12 in our case), L is the filter length (5 cm), M is the saturation magnetization of the matrix material (1.2 MA/m), B_0 is the applied magnetic flux density (0.7 T), η is the fluid dynamic viscosity (2 × 10⁻³ kg m⁻¹ s⁻¹), $r_{\rm pbp}$ is the radius of the particle buildup profile (which is initially equal to the radius of the wires, 30 μ m), and $v_{\rm f}$ is the mean fluid speed (2.0 mm/s). χ_i is the volume magnetic susceptibility of a cell of type i including the attached beads minus that of the fluid and is given approximately by

$$\chi_i = \left(\frac{2r_{\rm b}}{d_i}\right)^3 f c_i \chi_{\rm Fe} \tag{7}$$

where f is the volume fraction of a bead occupied by the magnetite (0.18), χ_{Fe} is the volume magnetic susceptibility of the magnetite (0.61), and c_i is the number of beads per cell of type i. Using (6) and (7) with $E_{\text{t}} = 0.95$ gives

$$c_{\rm t} = \frac{9\pi \log(20)\eta r_{\rm pbp}^2 v_{\rm f} d_{\rm t}}{2\langle h \rangle F L M B_0 r_{\rm b}^3 f \chi_{\rm Fe}}$$
(8)

which in our case, with $d_{\rm t}=10\,\mu{\rm m}$ and 50 nm beads, evaluates to 130 which is much less than $b_{\rm max}$. Thus we can safely assume that the linear regime applies and so $c_{\rm t}$ is proportional to n_0 . We may therefore write

$$Q \equiv -\log(1 - E_{\rm t}) \propto n_0. \tag{9}$$

The constant of proportionality depends on the bead capture probabilities β and γ which will differ among blood donors. We remove the effect of having a variety of blood donors by dividing Q by the constant of proportionality (calculated from the data obtained using cells of each donor using a regression line through the origin) to obtain the normalized quantity q which we therefore expect to obey $q = n_0$.

3. Materials and methods

100

105

110

115

120

125

130

135

140

145

3.1. Mononuclear cell preparation

Human peripheral blood was obtained from voluntary donors after informed consent and peripheral blood mononuclear cells were separated by density centrifugation by equal ratio (1:1) of blood to Lymphoprep (Axis-Shield PoC AS, Oslo) at 2000g for 20 min. Mononuclear cells (MNCs) at the interface were collected and resuspended in HGMS buffer (X-Zell Biotech Co. Ltd., Bangkok). MNC were counted using a haemocytometer (Boeco, Germany).

3.2. Isolation of CD3- and CD14-positive cells

A customized HGMS magnet, HGMS columns, HGMS buffers, and HGMS beads were from X-Zell Biotech Co. Ltd., Bangkok. The HGMS magnet provided a minimum magnetic field strength of 0.7 T between the poles, as determined by a DC-Gaussmeter (alpha-Lab Inc., Salt Lake City, Utah). Positive isolation of cells was performed according to the manufacturer's protocol. Briefly, MNCs were incubated with $100 \,\mu l$ of human AB serum (Gemini Bio Products Inc., California) for blocking of Fc receptors. Varying volumes of 50 nm or 100 nm anti-CD3 or anti-CD14 HGMS beads were added and the MNCs were incubated in HGMS buffer for 30 min at 4 °C. Cells were gently shaken every 10 min. The bead concentration was adjusted to between 1.5 and $13 \times 10^{12}\,\mathrm{beads/ml}$. The target cell concentration was between 0.75 and 20×10⁶ cells/ml. After incubation, cells were washed once with PBS (Biochrom AG, Berlin), pelleted at 400g for 10 min and resuspended in HGMS buffer. HGMS columns were filled with HGMS buffer in an upright position to evacuate air by upward displacement. After removing the remaining air bubbles by gentle finger tapping, a 20G/1-inch injection needle was connected to the stopcock. The column was placed between the poles of the HGMS magnet and equilibrated for 5 min. The stopcock of the HGMS column was opened, 10⁷ MNCs were applied for each experiment and the column was rinsed with 30 ml of HGMS buffer. After this, the stopcock was closed and the column was removed from the magnet. The column was flushed retrogradely with 12 ml of PBS. The eluate containing the target cells was collected, washed once by centrifugation at 1100g for 10 min, Giemsa stained, and analysed by light microscopy.

3.3. Phagocytic assay

To test the phagocytic activity of isolated CD14-positive cells, phagocytic assays were adapted from [11]. Briefly, 1×10^5 isolated CD14-positive cells were suspended in culture media (RPMI 1640 + 10% FBS) (both from Biochrom, Berlin) and incubated with 1×10^8 0.45 μ m-diameter latex beads in 24-well cell culture plates (Becton Dickinson, USA) at 37 °C and 5% CO₂. Phagocytic activity was analysed after 1.5 h. Cells were washed with 2% sucrose/PBS solution (USB Corporation, Cleveland/Biochrom, Berlin) to remove non-ingested latex beads (kindly synthesized for us by Prof. Pramuan Tungboriboonrat, Mahidol University). The entire protocol was performed under sterile conditions. After incubation, bead-containing and bead-free macrophages (MØ) were counted (per 1000 cells) under a phase contrast microscope (Olympus Optical Co., Tokyo) and their ratio calculated. After counting, isolated cells were subjected to cytospin, fixed and stained with Giemsa, and observed (at $400\times$ magnification) under a light microscope (Olympus Optical Co., Tokyo).

3.4. Parasite culture

Plasmodium falciparum strain AMB47 was cultivated in O-positive whole blood as described in [12]. Peripheral blood was obtained from voluntary donors and human serum from the blood bank of Ramathibodi Hospital, Bangkok. Blood was stored at 4 °C for at least one week to reduce viable leukocytes before parasite culture. Infected red blood cells (iRBCs) were cultured in malaria culture media (MCM) (10.43 g RPMI 1640 powder medium, 7.5% sodium bicarbonate (both Biochrom AG, Berlin), 40 μ g/ml gentamycin (Gibco), 25 mM 4-(2-hydroxyethyl)-1-piperazine ethane-4-sulphonic acid (HEPES) and 200 mM hypoxanthine (both from Sigma, Hamburg) supplemented with 10% non-inactivated human serum) in 75 cm² cell culture flasks (Corning Inc., New York) at 37 °C with 5% CO₂. The parasite culture medium was changed every 24 h. The culture was maintained in 5% haematocrit.

3.4.1. Synchronization of parasites

Parasites were synchronized to ring stages by treating with 5% sorbitol (Merck, Germany) following [13]. The parasite culture was washed twice (1000g, 90 s) with MCM after synchronization. Synchronized parasites in 5% haematocrit were then resuspended in MCM. Synchronization was evaluated by Giemsa staining.

3.4.2. Cryopreservation

For stock, 0.33 volumes of glycerolyte (Sigma, Hamburg) were added dropwise to packed iRBCs, mixed gently, and incubated at room temperature for 5 min. After incubation, 1.33 volumes of glycerolyte were added, frozen in cryovials (Corning Inc., New York) at -80 °C overnight, and then stored in liquid nitrogen.

3.4.3. Thawing

150

155

160

165

170

175

180

185

Cryovials were thawed at 37 $^{\circ}$ C and parasitized blood was transferred to 50 ml centrifuge tubes (Corning Inc., New York). 0.2 volumes of cold 12% NaCl (Merck, Darmstadt) solution were mixed gently with thawed iRBCs and incubated for 5 min at room temperature. Next, 10 volumes of cold 1.6% NaCl solution were added gently and centrifuged at 300g for 10 min at 4 $^{\circ}$ C. After removal of the supernatant, 10 volumes of cold 0.9% NaCl were added and mixed gently and centrifuged as above. The pellets were resuspended in MCM, and parasitemia and viability were measured by Giemsa staining.

3.5. Proliferation assay

Functional capacity of isolated CD3-positive cells was tested by proliferation and viability assays. The protocol was adopted from [14] with modifications. Briefly, MNCs were separated by Lymphoprep and cultured in a 75 cm² cell culture flask in 35 ml RPMI 1640 with 10% FBS at 37 °C in 5% CO₂ for 1.5 h. After incubation, supernatant containing suspended lymphocytes was removed. Monocytes attached to the flask surface were washed gently with 10 ml RPMI 1640 + 10% FBS. Finally, 5 ml of the same media was added to cover the monolayer of attached monocytes and incubated at 4°C overnight. On day 2, monocytes were removed from the pre-incubated cell culture flask by cell scraper (SPL Lifescience, Korea). HGMS isolation of CD3-positive cells was performed from MNCs obtained from peripheral blood of the same donor. Isolated monocytes and CD3-positive cells were counted by haemocytometer. Three experimental conditions were set per experiment. For all conditions, the initial cell count was 2×10^5 cells/well for MØ and 1×10^6 cells/well for CD3-positive cells. Cells were incubated in a 24-well cell culture plate (Becton Dickinson, USA) in 1 ml of media. Condition 1 comprised only MØ and unstimulated CD3-positive cells. In condition 2, P. falciparum iRBCs were used for stimulation of CD3-positive cells, as described in [15]. MØ were incubated with iRBCs for 4 h at 37 °C and 5% CO₂ before adding CD3-positive cells. Cell concentrations were set at 1:5:5 for MØ:CD3-positive cells:iRBCs, respectively. Condition 3 was identical to condition 1 except that CD3-positive cells were stimulated with $2 \mu g/ml$ leucoagglutinin (PHA-L) (Biochrom, Cambridge, UK). Proliferation and viability of CD3-positive cells was assayed at four different times (day 2, day 4, day 6, and day 8). Analysis was performed by Giemsa staining and light microscope. The entire protocol was performed under sterile conditions.

3.6. Mitotic assay

After counting CD3-positive cells, the remaining cells were incubated with $3\,\mu\rm g/ml$ cytochalasin B (Sigma-Aldrich, Germany) for 18–20 h at 37 °C and 5% CO₂ as described in [16]. After incubation, cells were harvested, subjected to cytospin, fixed for 10 min, and stained with Giemsa. Bi-, tri- and tetra-nucleated CD3-positive cells were analysed under light microscope. The mitotic index (MI), given by

$$\mathbf{MI} = \frac{\sum_{r=1}^{4} r n_r}{\sum_{r=1}^{4} n_r}$$

where n_r is the number of cells which are r-nucleated, was calculated from 1000 cells.

4. Results

190

195

200

205

210

215

220

225

230

4.1. Testing of predictive power of linear bead-capture theory

Predictive accuracy of linear bead-capture theory was examined with two different bead sizes and two different cell types, as described in the materials and methods. For both bead sizes, purities of CD3- and CD14-positive cells after magnetic separation were at least 95% in all experiments.

If values of $\log(1-E_{\rm t})$ are plotted against bead concentration n_0 then the theory predicts that the points should lie on a straight line through the origin. Experimental results were normalized as described in section 2.2. Data of q, the normalized value of $-\log(1-E_{\rm t})$, was combined from a total of 15 different blood donors and plotted against n_0 as shown in Figure 1. R^2 values range from 0.77–0.98.

For 50 nm beads, an $E_{\rm t}$ of over 80% was consistently achieved for bead concentrations $> 8.6 \times 10^{12} \,\mathrm{ml}^{-1}$ and target cell concentrations $> 4.0 \times 10^6 \,\mathrm{ml}^{-1}$ for CD14-positive cells, and for $> 6.0 \times 10^{12} \,\mathrm{beads/ml}$ and $> 10.4 \times 10^6 \,\mathrm{target}$ cells/ml for CD3-positive cells. For 100 nm beads, such capture efficiencies were obtained with $> 0.72 \times 10^{12} \,\mathrm{beads/ml}$ and $> 3.0 \times 10^6 \,\mathrm{target}$ cells/ml for CD14-positive cells, and $> 0.32 \times 10^{12} \,\mathrm{beads/ml}$ and $> 1.7 \times 10^6 \,\mathrm{target}$ cells/ml for CD3-positive cells (data not shown).

Morphological examination of isolated target cells (CD3- and CD14-positive cells) showed no discernible difference in their morphologies (Figure 2).

4.2. Functional assays

4.2.1. CD3-positive cells proliferation and mitotic assay

To demonstrate the viability of CD3-positive cells after HGMS, cells were subjected to proliferation assays. Figure 3 depicts the proliferation pattern of isolated CD3-positive cells. Experiments were continued over 8 days, with three different conditions as described in the materials and methods. Condition 1 (MØ and CD3-positive cells without stimulation) served as control and did not show significant proliferation at any time. In condition 2 (MØ + iRBCs + CD3-positive cells), proliferation of CD3-positive cells was seen from day 2 until day 6. The number of cells increased 1.5-, 2.4- and 2.8-fold on days 2, 4, and 6, respectively. A decrease in the number of cells was observed on day 8. With condition 3 (CD3-positive cells co-cultured with MØ stimulated with PHA-L), the number of cells increased 1.6-, 2.8- and 3.5-fold on days 2, 4, and 6, respectively. CD3-positive cell numbers decreased after day 6 (Figure 3).

MI of isolated CD3-positive cells is shown in Figure 3. MI for both conditions 2 and 3 was higher than controls. However, only MI for condition 3 was significantly higher than the control (p < 0.05). On day 6, over 80% of PHA-stimulated CD3-positive cells and 30% of iRBC-stimulated CD3-positive cells were binucleated as compared to 3% binucleated cells in the control. MI at day 2, day 4, day 6 and day 8 was, respectively, 0.97, 1.09, 1.41, and 0.89 for unstimulated CD3-positive cells, 0.98, 1.22, 1.74, and 1.13 for iRBC-stimulated CD3-positive cells, and 1.3, 1.54, 2.5, and 1.19 for PHA-stimulated CD3-positive cells (inset graph). Unstimulated CD3-positive cells showed hardly any proliferation and retained their cellular morphology and membrane integrity (inset picture with white arrow head). However, iRBC-stimulated (inset picture with yellow arrow head) and PHA-stimulated (inset picture with black arrow heads) CD3-positive cells showed clear binuclei on day 6. Cells with tri- or tetra-nuclei were also observed (pictures not shown). Fewer proliferating CD3-positive cells were found on day 2 and day 4 (pictures not shown).

4.2.2. Phagocytic assay

To test key functions of CD14-positive cells after HGMS, phagocytic assays were performed by latex bead $(0.45~\mu\mathrm{m})$ ingestion assay. Around 82% of cells showed ingestion of latex beads in 1.5 h. Phagocytosis was statistically significant (p < 0.01). A representative photograph of cells with ingested latex beads is shown in Figure 4. Identical results were observed after HGMS of CD14-positive cells with both 50 nm and 100 nm magnetic beads (100 nm bead data not shown).

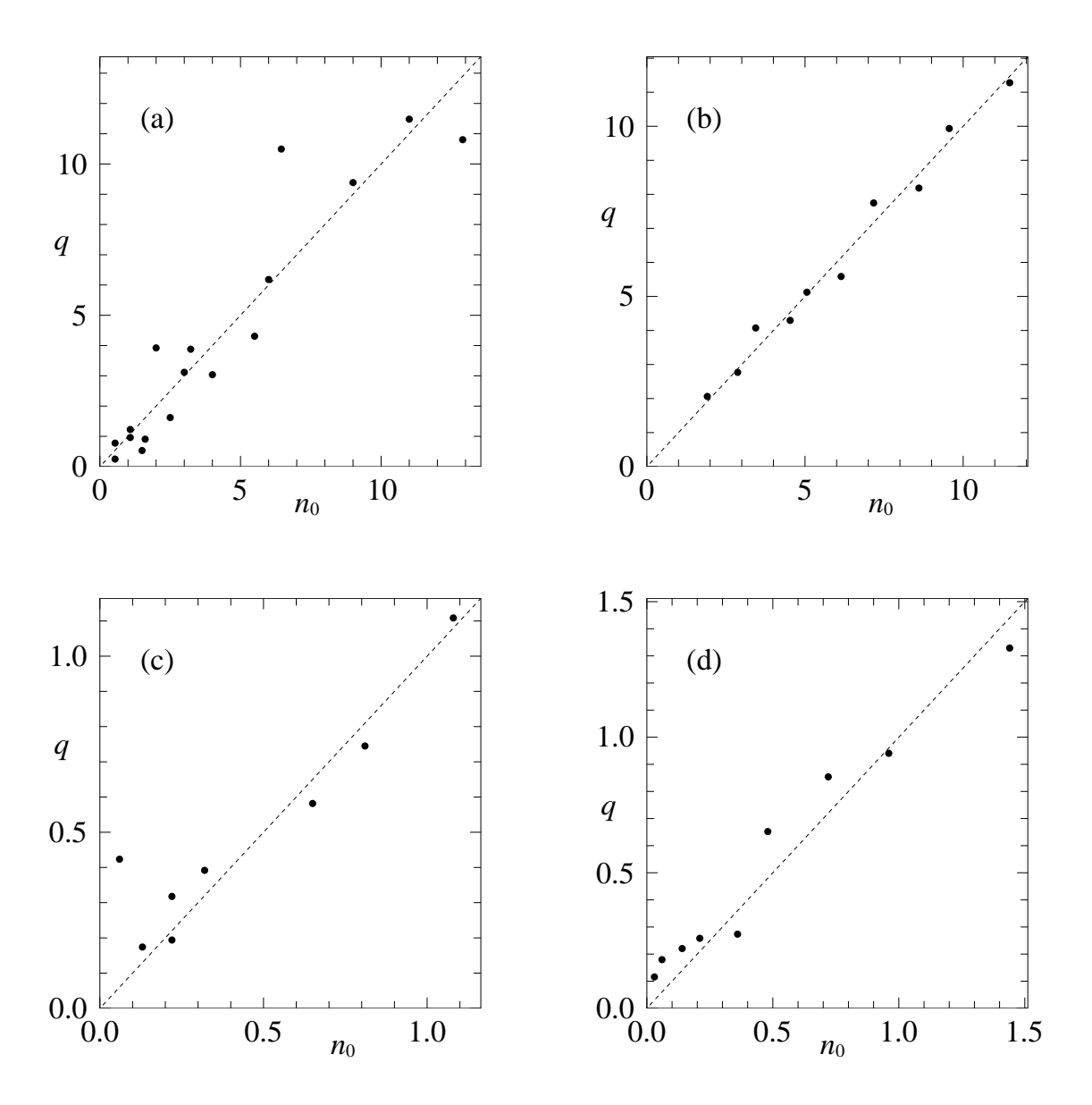


Figure 1: Normalized $-\log(1-E_{\rm t})$ against bead concentration n_0 (both in units of $10^{12}\,{\rm ml}^{-1}$) for both target cell types and bead diameters: (a) CD3 50 nm ($R^2=0.88$) (b) CD14 50 nm ($R^2=0.98$) (c) CD3 100 nm ($R^2=0.77$) (d) CD14 100 nm ($R^2=0.93$).

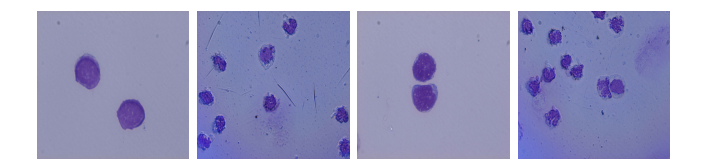


Figure 2: Morphologies of captured target cells. From left to right: CD3 50 nm; CD14 50 nm; CD3 100 nm; CD14 100 nm. Images in this and subsequent figures were taken at $400 \times$ magnification by light microscope.

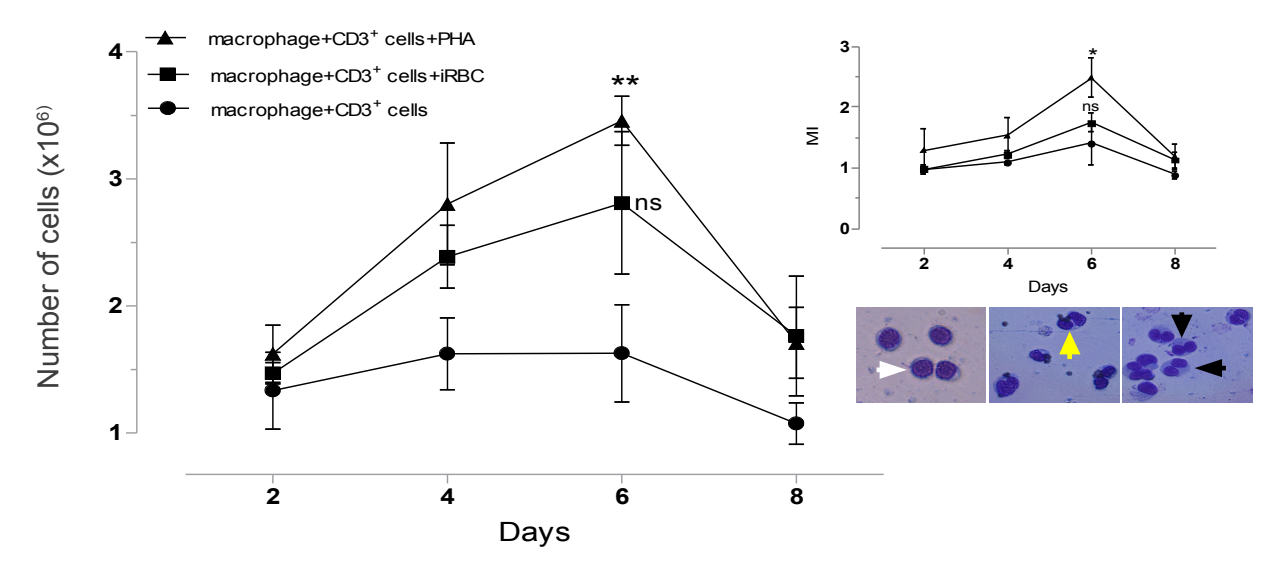


Figure 3: Functional analysis of CD3-positive cells isolated by HGMS with 50 nm magnetic beads by proliferation and mitotic assays. The MØ:CD3-positive cell:RBC ratio was set at 1:5:5 (iRBCs only in condition 2). Significant proliferation of CD3-positive cells was observed in conditions 2 and 3 (p < 0.01). For mitotic assays, the number of binucleated cells was counted. Representative morphology of binucleated CD3-positive cells is shown in the inset. (Giemsa stained slides of day 6 for all three experimental conditions). White arrow shows unstimulated CD3-positive cells, yellow arrow shows binucleated cells in iRBC-stimulated CD3-positive cells, and black arrows show binucleated CD3-positive cells in PHA-stimulated condition. Mitotic index (MI) for stimulated (with iRBCs and PHA-L) and unstimulated CD3-positive cells is shown in the inset graph. MI of CD3-positive cells stimulated with PHA-L was significantly higher than controls on day 6 (p < 0.05) compared to unstimulated CD3-positive cells on day 6. Data are collected from three independent experiments and calculated as mean \pm SE. ns = not significant.

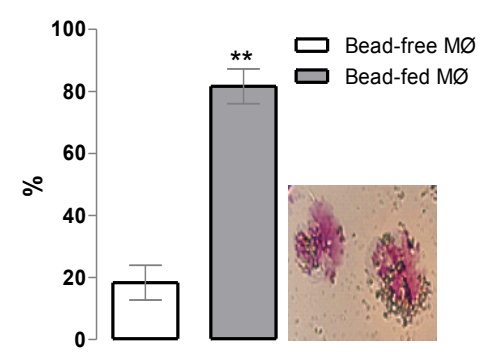


Figure 4: Phagocytic assay based on ingestion of latex beads $(0.45\,\mu\text{m})$ by CD14-positive cells-derived macrophages $(M\varnothing)$, after isolation by HGMS system with 50 nm magnetic beads. $M\varnothing$ (1×10^5) were exposed to latex beads (1×10^8) for 1.5 h in a 24-well cell culture plate and then observed under a phase contrast microscope. Percentages of bead-free (white bar) and bead-fed (grey bar) $M\varnothing$ were calculated from a total count of 1000 cells. $M\varnothing$ were also subjected to cytospin for Giemsa staining to see latex beads inside cells. Inset image: a representative photograph of bead-fed $M\varnothing$. Data are calculated from three independent experiments as mean $\pm SE$.

5. Discussion

235

240

245

250

255

260

265

270

275

280

In spite of the three decade-long history of HGMS in biomedical research, very few studies are available that examine the influence of physical parameters on capture efficiency $E_{\rm t}$. This seems surprising given that not only the key parameters (drag force and magnetic force) of a conventional HGMS apparatus can be considered constant, but also that the physical parameters of magnetically labelled cells vary only in a very narrow range. More specifically, cell size and receptor density are well characterized for a large number of cell sub-populations, and together with known parameters of the HGMS apparatus, it can be hypothesized that consistent separation results should be achievable. The present study developed linear bead-capture theory which identifies bead concentration as the single most important parameter to predict $E_{\rm t}$.

The study chose to focus on CD3-positive cells, which are fairly constant in both size and CD3 receptor expression [17], and CD14-positive cells which exist in two ranges of diameters, both with fairly constant CD14 receptor expression [11, 18, 19]. These two cell types, together with two different bead sizes, served as a model to test linear bead-capture theory on a generic, buffer-optimized HGMS system.

The theory predicts that $\log(1-E_{\rm t})$ is proportional to the number of beads bound to target cells. When the number of beads bound to target cells is small, this number of bound beads is in turn proportional to the initial concentration of beads during incubation of cells with beads. In other words, plots of $\log(1-E_{\rm t})$ against initial bead concentration n_0 for various bead and target cell concentrations are expected to lie on a straight line through the origin.

Results of the present study confirm that the theory predicts $E_{\rm t}$ in a highly significant manner, with R^2 values ranging from 0.77–0.98 (Figure 1). As predicted by linear bead-capture theory, it is clear that bead concentration and bead size must be optimized, while taking into account the surface receptor density of target cells, to achieve consistently high $E_{\rm t}$.

Interestingly, variation of bead and target cell concentration, or in other words, variation of the bead/cell ratio and $E_{\rm t}$ had no influence on isolation purity. Positive selection of CD3- and CD14-positive cells by the HGMS system led to over 95% purity in all experiments.

From the above, it should now become possible to better predict $E_{\rm t}$ for different cell types and bead sizes. For example, CD34-positive haematopoietic stem cells were described to have receptor densities of around 50 000 receptors per cell [20] or, in other words, around 2 times lower receptor density than CD3- and CD14-positive cells. At the same time it is known that $E_{\rm t}$ for CD34-positive cells in conventional HGMS systems are rather inconsistent [21]. It may now be hypothesized that commonly used protocols have not optimized the bead concentration during labelling of cells with beads and/or that commercially available 50 nm beads are not able to confer sufficient magnetic susceptibility to cells with such low receptor densities. In the latter case, use of 100 nm beads would increase magnetic susceptibility by one order of magnitude and should therefore lead to much more consistent results.

Since linear bead-capture theory might require different bead sizes for optimization of capture efficiency, the present study also examined the effect of varying bead diameters on cellular functions. HGMS-purified CD14- and CD3-positive cells were assessed by phagocytic and proliferation assays. Assays were performed without prior removal of beads, as is sometimes recommended [22].

Viability and proliferation rates of CD3-positive cells remained unchanged after separation with both 50 nm and 100 nm beads. Mitotic indices of CD3-positive cells were highest when stimulated with PHA-L, while stimulation with iRBCs resulted in lower, but still significant, mitosis. The latter does not seem surprising given the entirely different mechanisms of stimulation: PHA-L directly recruits T lymphocytes to undergo mitosis [23] whereas iRBCs are phagocytosed by monocytes and by antigens presented to T lymphocytes [24].

To examine functionality of CD14-positive cells isolated by HGMS, the inert latex beads ingestion model was adopted. Ingestion of latex beads in monocytes was previously explained as a measure of frustrated phagocytosis; over 80% of phagocytically active monocytes reflect optimal cellular engagement with inert latex beads [25, 26]. Results of the present study show that for isolation of CD14-positive cells with both 50 nm and 100 nm beads, over 80% of cells were phagocytically active. Also, it was observed that adhesion capacities of CD14-positive cells on cell culture dishes were over 80% (data not shown).

In summary, linear bead-capture theory predicts $E_{\rm t}$ in a highly significant manner. Assay-dependent optimization of bead concentration and bead size seems feasible since no change of cellular functions could be observed in HGMS-isolated cells labelled with paramagnetic beads of different diameters.

Further studies corroborating linear bead-capture theory are certainly warranted. For example, the theory contains various parameters whose values are difficult to obtain theoretically. The most important of these are the quantities $\beta\kappa$ and $\gamma\kappa$ which relate to the rate at which beads bind to the cells (see section 2.1). To further refine the predictive power of the theory by finding these values more directly, data on the number of beads attached as a function of time will be needed.

Acknowledgements and declarations

We thank Prof. Pramuan Tungboriboonrat, Chemistry Department, Mahidol University for synthesizing the latex beads. This study was supported by a Thailand Research Fund grant (BRG53_0052). The funding source had no involvement in the design of this study, collection, analysis and interpretation of the data, in writing the manuscript and in the decision to submit the paper to this journal. SCB is the director of a company developing HGMS systems for biomedical research. The other authors declare that they have no competing interests.

References

285

290

295

300

305

310

315

320

325

330

335

340

- [1] Øren A, Husebø C, Iversen AC, Austgulen R (2005) A comparative study of immunomagnetic methods used for separation of human natural killer cells from peripheral blood. *Journal of Immunological Methods* **303**, 1–10.
- [2] Oberteuffer JA (1973) High gradient magnetic separation. IEEE Transactions on Magnetics MAG-9, 303-306.
- [3] Paul F, Roath S, Melville D (1978) Differential blood cell separation using a high gradient magnetic field. British Journal of Haematology 38, 273–280.
- [4] Paul F, Roath S, Melville D, Warhurst DC (1981) Separation of malaria-infected erythrocytes from whole blood: use of a selective high-gradient magnetic separation technique. *Lancet* 318, 70–71.
- [5] Miltenyi S, Muller W, Weichel W, Radbruch A (1990) High gradient magnetic cell separation with MACS. Cytometry 11, 231–238.
- [6] Grutzkau A, Radbruch A (2010) Small but mighty: How the MACS-technology based on nano-sized supermagnetic particles has helped to analyze the immune system within the last 20 years. Cytometry 77A, 643–647.
- [7] Pappas D (2010) Practical Cell Analysis, Wiley.
- [8] Bhakdi SC, Ottinger A, Somsri S, Sratongno P, Pannadaporn P, Chimma P, Malasit P, Pattanapanyasat K, et al (2010) Optimized high gradient magnetic separation for isolation of Plasmodium-infected red blood cells 9, 38.
- Baier T, Mohanty S, Drese KS, Rampf F, Kim J, Schönfeld F (2009) Modelling immunomagnetic cell capture in CFD.
 Microfluidics and Nanofluidics 7, 205–216.
- [10] Gerber R, Lawson P (1989) The HGMS filter performance exponential law. IEEE Transactions on Magnetics 25, 3806–3808.
 - [11] Wang SY, Mak KL, Chen LY, Chou MP, Ho CK (1992) Heterogeneity of human blood monocyte: two subpopulations with different sizes, phenotypes and functions. *Immunology* 77, 298–303.
 - [12] Trager W, Jensen JB (1976) Human malaria parasites in continuous culture. Science 193, 673-675.
- [13] Lambros C, Vanderberg JP (1979) Synchronization of Plasmodium falciparum erythrocytic stages in culture. Journal of Parasitology 65, 418–420.
 - [14] Potter MR, Moore M (1975) PHA stimulation of separated human lymphocyte populations. Clinical and Experimental Immunology 21, 456–467.
 - [15] Scholzen A, Mittag D, Rogerson SJ, Cooke BM, Plebanski M (2009) Plasmodium falciparum-mediated induction of human CD25^{hi} Foxp3^{hi} CD4 T cells is independent of direct TCR stimulation and requires IL-2, IL-10 and TGFβ. PLoS Pathogens 5, e1000543.
 - [16] Yılmaz S, Ünal F, Yüzbaşıoğlu D (2009) The in vitro genotoxicity of benzoic acid in human peripheral blood lymphocytes. Cytotechnology **60**, 55–61.
 - [17] Ginaldi L, Matutes E, Farahat N, De Martinis M, Morilla R, Catovsky D (1996) Differential expression of CD3 and CD7 in T-cell malignancies: a quantitative study by flow cytometry. *British Journal of Haematology* **93**, 921–927.
 - [18] Ziegler-Heitbrock HW, Strobel M, Kieper D, Fingerle G, Schlunck T, Petersmann I, Ellwart J, Blumenstein M, et al (1992) Differential expression of cytokines in human blood monocyte subpopulations. Blood 79, 503-511.
 - [19] Passlick B, Flieger D, Ziegler-Heitbrock HW (1989) Identification and characterization of a novel monocyte subpopulation in human peripheral blood. *Blood* **74**, 2527–2534.
- [20] Civin CI, Handgretinger R, Urbano-Ispizua A (2004) Use of purified stem and progenitor cells for transplantation. In: Atkinson K, Champlin R, Ritz J, Fibbe WE, Ljungman P, Brenner MK (eds) Clinical Bone Marrow and Blood Stem Cell Transplantation, 3rd edn, Cambridge University Press, Cambridge, pp 226–249.
 - [21] Lang P, Schumm M, Taylor G, Klingebiel Th, Neu S, Geiselhart A, Kuci S, Niethammer D, et al (1999) Clinical scale isolation of highly purified peripheral CD34+ progenitors for autologous and allogeneic transplantation in children. Bone Marrow Transplantation 24, 583–589.

- [22] Lea T, Smeland E, Funderud S, Vartdal F, Davies C, Beiske K, Ugelstad J (1986) Characterization of human mononuclear cells after positive selection with immunomagnetic particles. *Scandinavian Journal of Immunology* 23, 509–519.
- [23] Winkelstein A, Simon PL, Myers PA, Weaver LD (1986) Comparisons of 12-tetradecanoylphorbol-13-acetate (TPA) and PHA as mitogens in the T-lymphocyte colony assay. *Experimental Hematology* 14, 1023–1028.
- [24] Bettiol E, Van de Hoef DL, Carapau D, Rodriguez A (2010) Efficient phagosomal maturation and degradation of Plasmodium-infected erythrocytes by dendritic cells and macrophages. Parasite Immunology 32, 389–398.

345

350

- [25] Henson PM (1971) Interaction of cells with immune complexes: adherence, release of constituents, and tissue injury. Journal of Experimental Medicine 134, 114–135.
- [26] Takemura R, Stenberg PE, Bainton DF, Werb Z (1986) Rapid redistribution of clathrin onto macrophage plasma membranes in response to Fc receptor-ligand interaction during frustrated phagocytosis. *Journal of Cell Biology* 102, 55–69.